STUDIES ON MAGNETIC THIN FILMS PREPARED BY IONIZED CLUSTER BEAM TECHNIQUE

NAOTO KONDO

PREFACE

Recently,metallic compound materials for magnetooptical memory devices have been proposed. Because of their inherent properties such as high recording density and no necessity of mechanical motion, thin films of these materials have been studied intensively.

On the other hand, there has been much interest in the research and development of thin film devices by "Ion-Based Technique", since the film growing process was found to be intensified in the presence of charged particles and the kinetic energy of the source materials. Applying the ion-based technique to film formation, the film properties such as crystallographic, optical, electrical and magnetic properties can be easily controlled by adjusting growth and/or deposition conditions.

In this thesis, intermetallic magnetic thin films prepared by the Ionized Cluster Beam (ICB) technique are investigated with respect to their crystallographic and magnetic properties. The ICB technique was originally developed by Professor Toshinori Takagi, Department of Electronics in Kyoto University. In these days, this technique has been widely spread over a number of research group and utilized intensively in many kinds of device formation. The author hopes that the studies in this thesis will stimulate the magnetic thin film device development.

March 1985

Naoto Kondo

ACKNOWLEDGEMENT

The author wishes to express his deep appreciation to Professor Toshinori Takagi who instructs him to fundamental attitudes of research implementation and guide him to great extent in research and also gives him invaluable advices. The author absolutely wishes to express his gratefull thanks to Professor Kakuei Matsubara in Yamaguchi University for intimate advices and encouragement in whole his Kyoto University days and for inviting him to such a intresting study. The author is gratefull to Professor Akio Sasaki, Professor Akira Kawabata and Associate Professor Isao Yamada for their stimulating discussions and valuable suggestions on his research.

Grateful appreciation is due to Dr. Hiroshi Takaoka and Dr. Junzo Ishikawa for encouragement and useful advices throughout his research. The author is indebted to Mr.Hiroshi Tsuji and Miss Fumiko Kiuchi for continuous encouragement. The author is also indebted to the members of Professor Takagi'sResearch Group for installing new fashion to make new concepts in material physics. The author acknowledges a technical support by Osaka Koon Co., Ltd.

Finally, the author should manifest his appreciation to his late father who had been watching his direction in silence until he decided to go to the postgraduated course of Kyoto University.

Thanks are also to Kyoto, "Daimonji no Okuribi", "Shiden", "Higashiyama" that are still in the author's mind.

CONTENTS

LIST OF FIGURES

LIST OF TABLES

I INTRODUCTION

At the present of development in computer technology, there is an increasing need for improvement in the speed and capacity of the mass storage technology. Although the main memory in a computer is being replaced by semiconductor devices, magnetic recording techniques continue to dominate in the area where large storage capacity and nonvolatility are required. Furthermore, if a large mass memory can have the access time more compatible to the cycle time of the central processing unit, the complex hierarchy of the memory and storage devices and the associated interface electronics employed at the present time can be vastly simplified. The main limitation of the present magnetic recording technology lie in the achievable recording density and the required relative mechanical motion. The recording density is not limited by the resolution of the medium but rather by practical engineering considerations such as the signal-to- noise ratio (S/N) and difficulty in rapid and accurate positioning of the inductive transducer with respect to the medium. The requirement of mechanical motion not only limits the speed but also reduces the reliability. It is these areas of weakness of the conventional magnetic recording that optical technology can offer an improvement. Utilizing optical effects in material medium to derive the read out signal from the stored infomation, the signal is not limited by the bit stored enegy but by the tolerable read beam intensity. In fact, information bits of optical diffraction limited size have been written, erased, and read with adequate S/N. Addressing by optical beam

does not necessarily involve mechanical motion if inertialess beam deflection and modulation are utilized. Since the recording transducer and medium are linked by an optical beam at a distance, there will be no mechanical contact or wear and, therefore, improved reliability. The advantages of the magnetic recording technology and optical technology are thus combined in the magnetooptical memory. In order effectively to utilize the optical beam for addressing, however, new read-write physical effects and materials must be explored.

There proposed some metalic compound materials for magneto-optical memory devices, such as MnBi[1)-7)], rare earth-transition metal (RE-TM) alloy[8)-14)], prepared by the conventional methods involving the vaccum evaporation, sputtering, etc. There exist, however, some problems to be solved with respect to each material, such that uniformity over large surface area is unlikely to be achieved in case of MnBi films and that the magnetic anisotropy perpendicular to the film surface could not be controllable because the origin of the perpendicular anisotropy has not been clarified in case of RE-TM alloy thin films, and so on.

Recently there has been much interest in the reseach and development of thin film devices by "Ion-Based Technique", since the film growing process was found to be intensified in the presence of charged particles and the kinetic energy of the source materials. The object of ionization is to utilize the inherent properties of materials by giving some kinetic energy through the ionization process. Chemical activity includes the film formation activity and the enhancement of the chemical

reaction by ionization. The presence of the ionezed particle in the evaporated materials, even without acceleration of the ionized particles, greatly influences the critical parameters of the condensation process for the film formation. Moreover, adhesion strength, packing density, surface morphology, crystalline state and structure of the deposited films, or efficiency of synthesis of deposited compound materials, etc. are improved remarkably by the acceleration of the ionezed particles[15)-20)].

From the standpoint that the ionization of the material is only a step to provide them with some kinetic energy or to enhance their chemical activity, it is not always necessary to ionize each atom and/or all of the atoms if ionized vapour aggregates, i.e. cluster can be produced. Based on this idea, the Ionized Cluster Beam (ICB) technique was proposed by T.Takagi in 1972 [21)]. Clusters which consist of about 500 - 2000 individual atoms loosely coupled together are generated by an adiabatic expantion of the vapourized material through a nozzele. Several tens per cent of these clusters are ionized by electron bombardment and are accelerated to a substrate surface. Both ionized and neutral clusters are broken up into atoms and are scattered over the surface (migration effects), resulting in a great improvement in the crystalline state of the deposited film. In addition to the general effects of accelerated ions in the ion-based technique, the enhanced migration effect of adatoms after bombardment of the clusters on the substrate surface is one of the most important characteristics of this tech-

nique [22), 23)]. As an ionized cluster is always singly charged, i.e. only one atom in a cluster is ionized, ionized clusters possess a small charge-to-mass ratio, which reduces the charging up of the insulator substrate due to an accumulation of positive charge and also eliminates problems caused by space charge repulsion in high current ion beam transport [24)].

In this thesis, thin films of compound materials for magnetooptical memory application are prepared by using the ICB technique and the crystallographic and magnetic properties of films are described.

Chapter II describes the concept of thermomagnetic recording though which the information is written or erased in magnetooptical memory and material requirements for magnetooptical recording are also described with respect to read, write and erase process.

Chapter III deals with the outline of the ICB and descrives the characteristics of the practical ICB source used in preparing films concerning with this thesis.

From Chapter IV to Chapter VI, films of MnBi, MnNiBi and GdFe are investigated in detail.

Chapter VII provides the concluding remarks of this thesis.

II MAGNETOOPTICAL RECORDING

2.1 Introduction

Considering magnetooptical recording, the basic advantage in using an optical beam for addressing and heating source lies in the following factors:

1. Addressing resolution is the diffration limited spot size. 1 μm bit dimensions are conveniently achievable, resulting in an anticipated packing density in excess of 10^8 bits/cm^2, at 2 μm center-to-center spacing.
2. With an optical beam for addressing, the readout signal is derived from the beam intensity, which is external to the memory bit. Thus, high readout S/N together with high packing density is possible.
3. Addressing speed is limited by the speed of deflection of the beam with respect to the memory medium. Since an optical beam is inertialess, much improved access time is now possible [28], and the electronic bandwidth of the servo loop can be realized.
4. The optical transducer is maintained at a distance of the final lens focal length away from the memory medium. This can be order of magnitude increase from the tranceducer-medium apacing required for conventional inductive recording. Therefore, the head crash problem is completely eliminated.
5. Optical beams are especially suited for parallel processing addressing, new approaches of memories such as

the holographic recording technique are made possible.

The realization of optical addressing in magnetic recording requires the development of read, write, and erase technology as well as new systems approach.

2.2 Thermomagnetic Recording

The writing and reading techniques in either digital or holographic systems are identical in principle. The writing process is called thermomagnetic writing, which may be defined as the creation of an image on the magnetic medium by first heating above ambient temperature and then cooling the medium in a magnetic field. Although several different techniques based on different magnetic phenomena may be used, the three most common techniques are the following: (1) Curie point writing, in which the area of interest is heated above the Curie temperature and subdequently cooled either with or without a bias magnetic field. A bias field is not required if the demagnetizing field due to the unheated regions is large enough to produce an area of reversed magnetization and hence produce the desired image. (2) Compensation point writing, in which ambient temperature is normally selected to be slightly above the compensation temperature. The coercive force has been reduced with increasing temperature due to the compensation of the sublattice magnetizations and sufficiently for an reversed bias field to produce the image. (3) Reduced coercive field writing, in which the heated area is raised to a temperature below the Curie temperature. The large decrease in the coer-

cive force at this temperature is then utilized as in compensation point writing.

1. Curie Point Writing

The term "Curie point writing" was first proposed by L.Mayer [29] in 1958 to describe thermomagnetic recording in MnBi films. Curie point writing is a method in which the temperature rise in the heated spot exceeds the Curie temperature of the medium. During cooling from the Curie temperature, the magnetic closure flux as well as the applied external field can effectively determine the direction of magnetization of the heated bit, In a medium of thin film form with easy direction of magnetization perpendicular to the film plane, the closure flux is in the direction opposite to the magnetization direction. For this case, writing from the surrounding 0 level to a 1 level requires no external field. The erasure operation involves application of an external field to overcome the demagnetization field to effect the written bits to be erased back to the 0 level.

In order to be able to erase a spot effectively without affecting the unheated region, one condition must be satisfied: the demagnetization field must be less than the coercive force of the medium.

2. Compensation Temperature Writing

In certain ferrimagnetic material such as gadolinium iron garnet (GdIG), gadolinium cobalt and gadolinium iron alloys the two sublattice magnetization are in opposite directions. At certain temperature, called the compensation temperature, the

magnitude of these sublattice magnetizations cancel out each other and the medium attains extremely high coercivity H_c. A few degrees away from this compensation temperature the coercivity drops and magnetization switching becomes easy. This is the basic mechanism for the compensation point writing technique. By operating the medium at the compensation temperature, a switching field is applied in coincidence with a laser heating pulse, which allows the heated spot to raise above a temperature at which the coercivity is below the applied switching field. The heated spot can therefore be switched in one direction or the other determined by the applied field. This method of writing has been experimentally demonstrated in single crystals [30] and thin films [31] of gadolinium iron garnet, and thin films of gadolinium cobalt [14].

The reading process is accomplished by either transmission or reflection of light [32)-34)]. Utilizing polarized light, the former is called the Faraday effect and the latter is called the Kerr effect. Several magnetooptical effects could be used, but the polar Faraday and the polar Kerr effects are the largest. The Faraday effect results from an interaction of the light with the magnetization, which causes a rotation of the plane of polarization of the light. This rotation F(in deg/cm) is proportional to the path length and to the magnitude of the magnetization component which is parallel to the direction of light propagation. An area with reversed magnetization direction consequently reverses the sense of the Faraday rotation. The Kerr effect is analogous and arises from an interaction of

the light vectors and the magnetization direction at the media surface. Depending on the system configuration, either effect may be used.

The writing process involves heating and, for an unsupported film, sinple considerations show the required energy to be proportional to the product of the specific heat with the neccessary temperature rise divided by the optical absorption coefficient α. For a supported film, the situation is more complicated. A one-dimensional calculation has shown, that as a result of significant thermal diffusion into the substrate during heating, there is an optimum film thickness for thermomagnetic writing and that this thickness depends on the thermal properties (specific heat, thermal conductivity) of both the film and substrate as well as α [35].

The optimum thickness for maximizing the readout signal in the transmission mode is not identical to the desirable thickness for maximizing the writing process. The film must be thick enough to maximize F, but thin enough so that the light used for reading is not totally absorbed. A simple factor $2F/\alpha$ has been traditionally chosen as a figure of merit since the maximum amount of detectable F is achieved in one optical absorption length. This figure of merit has been related to the achievable S/N ratio [32]. Recent investigations indicate this figure of merit is not totally sufficient,[36] but for the present study this oversimplified expression is used to give an estimate of the relative signal which can be obtained from diffent materials.

2.3 Material Requirement for Thermomagnetic Recording

The detailed requirements on materials for magnetooptical recording depend on the particular techniques utilized for read, write, and erase. However, the fact that the basic physical phenomena for readout is the magnetooptic effect and for writing-erasing is the thermomagnetic effect allows us to make a general assessment of the material requirements. In optically addressed systems, where the detection of the rotation of the plane of polarization is the signal, a large Faraday constant is required. Very low absorption of the beam would yield a maximum signal, but then it is more difficult to heat the material if the same wavelength is used for writing. It is commonly accepted that $2F/\alpha \simeq 1°$ is required for adequate readout. Since in all materials, α and F depend on temperature and wavelength, it is important that the required values for α and F are achievable at room temperature and in the convenient visible laser wavelength region.

The normal orientation of magnetization in general results in a smaller domain size, and therefore higher recording density. This normal orientation of magnetization relative to the film plane suggests that large positive values of uniaxial magnetic anisotropy are required. That is if $H_a = 2K_u/M_s$, then $H_a > 4\pi M_s$, where K_u is the uniaxial anisotropy constant and $4\pi M_s$ is the demagnetizing field of the thin film. Of course the thin film must be prepared with the easy magnetization axis oriented normal to the film plane. This is one of the most severe and important requirements.

Since it is impractical to confine an applied magnetic field to an area of the memory bit, the switching field normally covers a much larger area. The optical beam is used to select the micrometer size bit to be heated within this area. It is therfore important to have the switching field well below the medium coercivity H_c, so that the surrounding film is not switched. In the thin film case, H_c is nearly inversely proportional to the film thickness. Thin films are preferred from the coercivity consideration. In a magnetic medium where the hysteresis is not essentially square, the remanent magnetization can be perturbed by the presence of the external field even at values well below H_c. Since the magnetic field is present if neighboring bits are being written or erased, this field can cause the unheated bits to follow a minor loop, leadind to partial demagnetization and reduction of readout signal. If the medium possesses a square hysteresis loop, or one that shows essentially constant magnetization independent to the applied field with a magnitude below H_c, there is no danger of losing the remanent magnetization. This ensures the full readout signal of the stored information.

The minimum bit size that will be stable is a function of the material parameters. Minimization of the total free energy in a magnetized spot has been evaluated by R.Cohen and S.Mezrich [37]. The influence of the magnetic film parameters on the domain size, for a film thickness much greater than the spot diameter, is given by the approximate expression

$$d = \frac{(2\pi^3 t)^{1/2}}{4M_s} \left(\frac{kT_c K_u}{2ra}\right)^{1/4} \qquad (2.1)$$

where d is the domain diameter, t is the film thickness, r is the number of interacting neighbour bits, and a is the lattice constant. For example, with a 1000 Å thick MnBi film, the calculated minimum size spot is 1000 Å which would allow a density of 10^{10} bits /cm^2. In practice a realistic spot size is slightly less than 1 μm, but even this implied bit density (10^8 bits/cm^2) is not realizable because of the spreading of the heat in the plane of the film during writing. A practical bit density is about 10^6 bits/cm^2. Such high bit densities place stringent requirements on the uniformity of the film for bit-by-bit addressed memories.

III IONIZED CLUSTER BEAM TECHNIQUE [21)-24), 38)-55)]

3.1 Introduction

The Ionized Cluster Beam (ICB) technique has been developed by T.Takagi et al. A schematic diagram of these sources is shown in Fig.3.1.

For the ICB deposition, metal or semiconductor vapour to be deposited is ejected into a high vacuum chamber through the small nozzle of a special crucible in which material is vapourized at high temperature. The temperature of the crucible is controlled to maintain the optimum vapour pressure, usually 10^{-2} to several Torr. The clusters are formed by super condensation phenomena due to the adiabatic expansion through the nozzle. The clusters contain 500 - 2000 atoms loosely coupled together, which is different from the droplet (liquid particle) in that the droplet contains 5×10^8 - 5×10^9 atoms per droplet closely coupled to each other [56)-60)]. The clusters are ionized to be singly charged by electron bombardment in the ionization electrode assembly located above the crucible. The cluster ions are accelerated toward the substrate by a negative high potential applied to the accelerating electrode. Besides the ionized clusters, neutral clusters which remain unionized during flow in the ionization region move toward the substrate at a ejection velocity and without acceleration by the applied voltage.

Compared with other atomic- or molecular-ion-based techniques such as sputter deposition, ion plating, etc., one of the

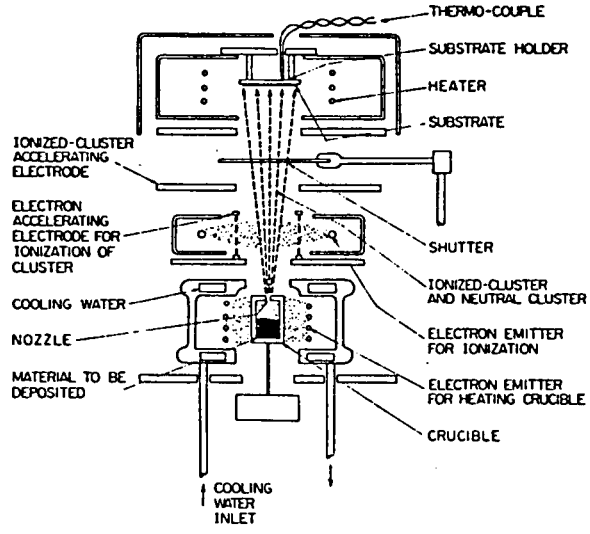

Fig. 3.1 A schematic diagram of the ICB source.

attractive features of the ICB technique was as follows: When the cluster is broken at its arrival on the substrate, each atom of the cluster has an average energy per atom of $\bar{E} = QV_a/N$, where Q is the electric charge, V_a is the acceleration voltage, N is the cluster size (number of atoms in a cluster). By controlling V_a, it is possible to provide each atom with an energy high enough for surface diffusion ($\bar{E} \simeq 1$ eV) but not sufficient for inducing defects in the layer ($\bar{E} < 5$ eV). By monitoring the electric current, it can be shown that although the charge on the cluster is sufficient to influence film formation, the actual electric charge content in the total cluster is very low. These features open the energy range of 1 to 20 eV per atom to investigation, whereas space-charge spreading effects require the accessible energy range to be as high as possible for deposition using charged atomic or molecular ions to ensure proper beam focusing and the maximum intensity [53].

From the fact mentioned above, the ICB technique seems to be very promising for the deposition of the intermetalic compounds concerned with this thesis. Moreover the reactive ionized cluster beam (R-ICB) technique, which is a modified one of the ICB technique to combine the source material with reactive gas, will be useful for the deposition of solid and gas phase materials to be required for a magnetooptical memory material in a future.

For each ICB and R-ICB type, a single and a multiple crucible system can be considered. The single crucible system is available for the deposition of a single element and some

compound materials, whose vapour pressures are almost equal. The multiple crucible system is used in the case that the vapour pressure of the composite element is different.

In this thesis, the multiple crucible system is used to obtain a stoichiometric composition because the vapour pressure of the composit e.g. Mn and Bi, Gd and Fe, differs so large that the reproducibility of film formation could not be achieved with a single crucible system.

3.2 General Description of The ICB System

3.2.1 Generation

A cluster source used is a cylindrical nozzle source. The dimensions and factors for design of the cluster source are different from those of molecular beam source as follows: The cluster grow by collisions with the surrounding vapourized atoms in the nozzle region, where the nozzle diameter D has to be larger than the mean free path λ of the atoms in the crucible. In order to make the adiabatic expantion more effective, the nozzle diameter is reduced to satisfy the condition that the ratio of the inner pressure P_0 of the crucible to the vapour pressure P outside the crucible is larger 10^4, and it is also desirable for D to be larger than the nozzle thickness L, that is, $L/D < 1$. A simple nozzle shape, e.g. a cylindrical type with a diameter D = 0.5 - 2.0 mm is found to be enough to form a cluster beam with a high drift velocity [61].

The range of the source temperature necessary to obtain

the required pressure P_0 for several materials is listed in Table 3.1. These are determined from the inner pressure P_0 in the crucible corresponding to 10^{-2} and 10 Torr., respectively. Since the source temperature in the ICB technique is required to be higher than that used in the conventional methods, the technique of the direct resistive heating of the source or of heating by electron bombardment are used in heating of the crucible.

3.2.2 Ionization

The cluster beam is ionized mostly to be singly charged by electron bombardment. The ionization energy of a cluster is estimated to be somewhat lower than that of the single atom but higher than the work function of the bulk material of the same element, since the binding energy of an electron is considered to be reduced by the interaction between the condensed atoms. Further, a cluster has a much larger ionization cross section, and it increases as about $N^{2/3}$ for larger clusters ($N > 50$) [62]. Therfore, a cluster is effectively ionized by electron bombardment. The electron current for ionization of 0 - 500 mA is found to give the ionization ratio of 0 - 50 % [44].

Figure 3.2 shows the ionization part of the ICB apparatus. The height h' of the electron accelerating electrode is designed to be so large ($h' > a$) that the high electric field to accelerate the clusters does not influence the electron current for ionization. In addition, the filament which emit electrons for ionization are designed to be in a square shape in order to

Table 3.1 Source temperatures for cluster source: T_r and T_h are temperatures corresponding to 0.01 and 10 Torr of inner pressures in the crucible, respectively.

Material	T_r(K)	T_h(K)
Mn	1210	1695
Bi	945	1350
Ni	1800	2430
Cu	1530	2140
Gd(est.)	1600	2220
Fe	1750	2390

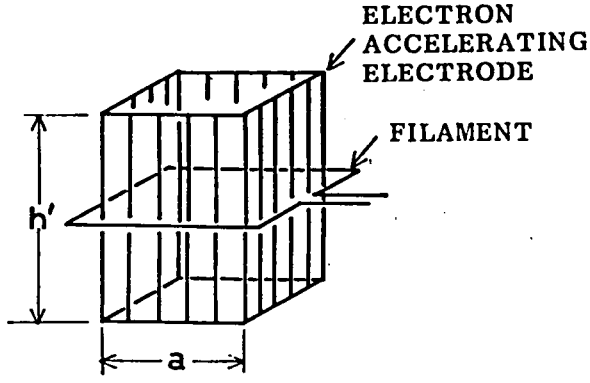

Fig. 3.2 Schematic diagram of the ionization part.

avoid radial concentration of the electrons which would occur with a circular filament. The square geometry results in spatially uniform ionization of the cluster beam, which is desirable to obtain a uniform film. [44),63)]

3.2.3 Acceleration

The ionized clusters are accelerated by the high electric field toward a substrate and deposited on it. The optimum acceleration voltage depends on other deposition parameters such as the substrate temperature and especially with the crystal structure which determines the epitaxial growth.[15),64)]. For example, the epitaxial growth of Si on Si substrate was achieved at acceleration voltage V_a of 6 kV (at the substrate temperature T_s = 620°C) [22)], likewise epitaxial films of Si on sapphire [34)], InSb on sapphire, and GaAs substrate were obtained at V_a = 4 kV (T_s = 760°C), V_a = 4 kV (T_s = 400°C), and V_a = 4 kV (T_s = 550°C), respectively [42)]. The epitaxial growth of ZnO on sapphire was obtained at V_a = 1 kV (T_s = 230°C) using the R-ICB technique, where reactive gas is combined with the standard ICB [15),49)].

On the other hand, for the c-axis oriented film growth of MnBi, ZnO and BeO onto an amorphous substrate, additional acceleration voltage was not necessary[49)-51)]. Good quality films showing a hexagonal structure could be obtained using the energy corresponding to the ejection velocity of the clusters alone. In addition, because a cluster has about a thousand times larger than that of an atom, it should be noted that even for

the acceleration potential of a few kV, the energy of each atom is still only in the order of a few eV. No space charge forces have been observed which affect the transport process of the clusters. This can be explained by the small charge-mass ratio and the short distance ($\sim$15 cm) from the cluster ion source to the substrate.

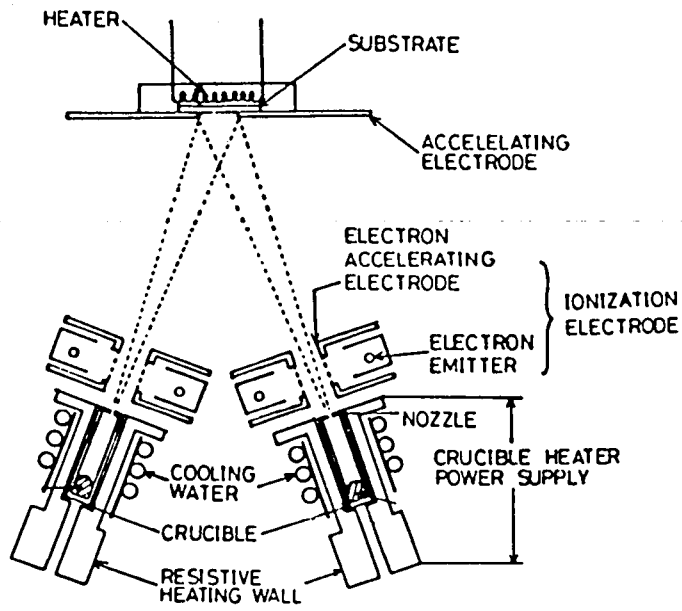

Fig. 3.3 Schematic diagram of the ICB source with the multiple crucibles.

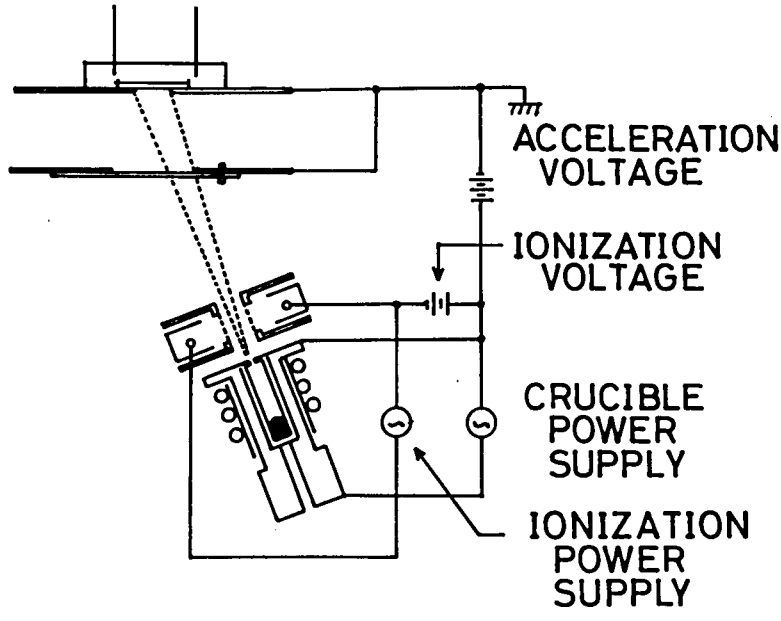

Fig. 3.4 The potential layout and power supplies of the ICB source.

3.3 Characteristics of the ICB System

In this section, the characteristics of the practical ICB used in preparing films are described in a case of Mn and Bi sources by way of example.

3.3.1 The ICB System used in this Study

The multiple crucible system was employed in order to make the cluster beams of materials having the vapour pressures different, as mentioned previous section. Figure 3.3 shows the schematic diagram of the deposition system, in which two ion sources are assembled to cross the cluster beams on the substrate surface. Each beam reaches the substrate at an angle of 16° to the substrate normal. In this apparatus, the substrate is held at ground potential in order that the acceleration voltage of each material can be controlled individually. The potential layout and power supplies are illustrated in Fig. 3.4.

The chamber is evacuated with a 6" oil diffusion pump (1200 l/sec) backed with Liq. N_2 cold traps, water cooling baffles and a rotary pump. Typical base pressure for this deposition chamber is 4×10^{-6} Torr. The operating pressure during deposition was typically $6 \sim 8 \times 10^{-6}$ Torr. Detailed assemblies of each part of the ICB system are described in accordance with the previous section.

A crucible and a resistive heating wall are made of dense and high purity graphite (apparent density 1.7 g/cm^3, ash content 20 ppm.), as shown in Fig. 3.5. The crucible was heated

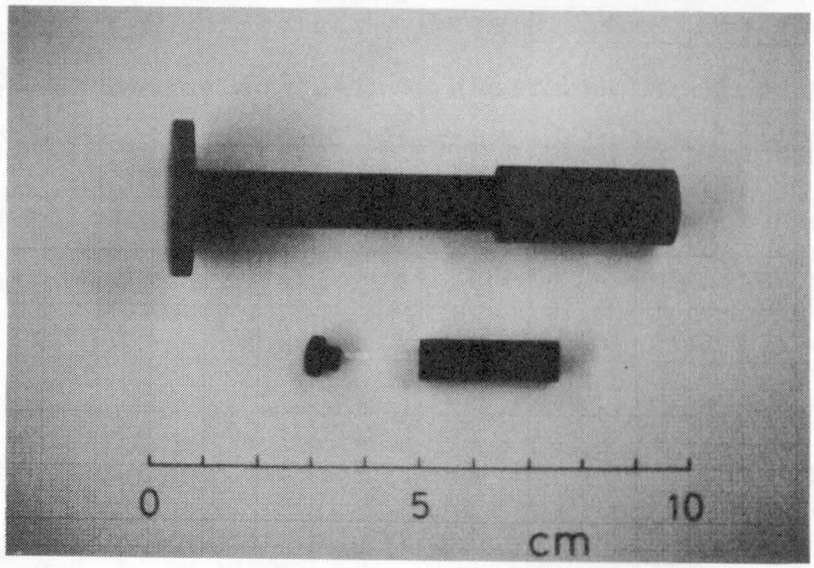

Fig. 3.5 A crucible and a resistive heating wall used in the ICB source.

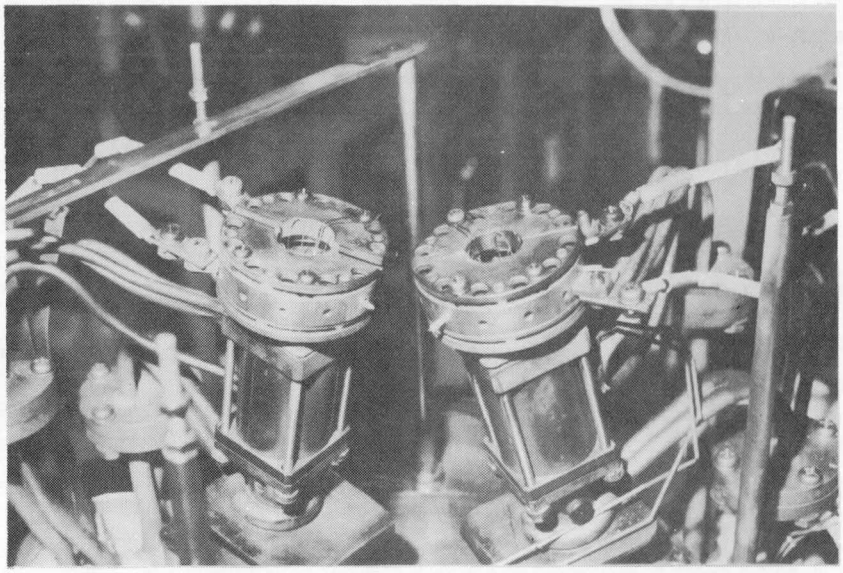

Fig. 3.6 The view of the ionization units of the ICB source.

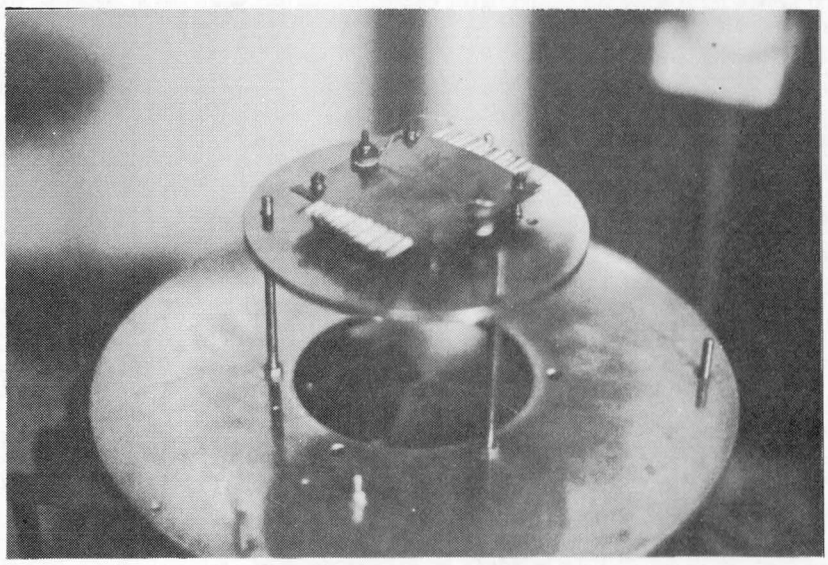

Fig. 3.7 The view of the substrate holder, the crucible heater, the acceleration electrode and the shutter.

by the direct current heating of the wall, and the temperature of the wall was measured with an optical pyrometer or an thermocouple brought into direct contact with the wall, when the temperature was needed not so high (Bi:∿ 900°C). The temperature reaches 1800 °C when the wall is supplied with a current of 250 A. The resistive heating wall is surrounded by radiation shields made of tantalum plate (thickness 0.1 mm), water cooled copper pipes and copper blocks (thickness 2 mm) in order to avoid the problems caused by the heat radiation.

The filament which emits electrons for ionization and the electron accelerating electrode are made of tungsten wire of 0.5 mmϕ and 0.4 mmϕ, respectively. These ionization elements are supported in a SUS blocks, as shown in Fig. 3.6, in which the ionization units are mounted on the copper blocks of crucible units.

The substrate holder is held at ground potential as well as the acceleration electrode, and over which the substrate heater made of tantalum wire (0.6 mmϕ) with an Al_2O_3 (alumina) insulator is assembled together, as shown in Fig. 3.7. The substrate temperature can be raised up to 400°C and measured by a chromel-alumel thermocouple.

3.3.2 Characteristics of the ICB System

This section describes the deposition rate, the ion current (I_i) and their spatial distribution with employing an acceleration voltage (V_a), an electron current for ionization

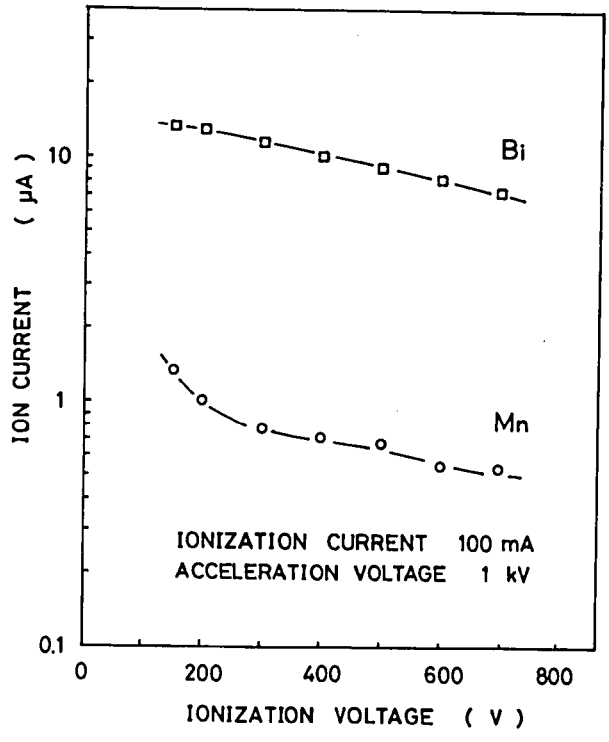

Fig. 3.8 Dependence of the ion current I_i on the ionization voltage V_e.

(I_e) and an ionizatin voltage (V_e) as parameters. The ion current I_i was measured with only a aluminum plate (40 mmϕ) and there are some overestimate caused by the secondary electron emitted from the plate in the obtained value of I_i.

Ion current of Mn and Bi clusters were measured at the condition that Mn was heated at 1650 °C, Bi 850 °C and the nozzle diameter were 0.6 mmϕ(Mn), 0.4 mmϕ(Bi). Figure 3.8 shows I_i as a function of V_e with I_e = 100 mA and V_a = 1 kV. For both case of Mn and Bi, I_i decreases monotonically with increasing V_e, and this tendency is similar to the ionization characteristic of mono atom except for the region below V_e = 200 V. Figure 3.9 shows the relation between I_i and I_e with constant V_e = 200 V and V_a = 1 kV. For both Mn and Bi, I_i increases monotonically with increasing I_e, which is predicted from the following equation.

$$N_i = N_0 \cdot \Omega(E_b) \cdot V_b \cdot n_b \cdot \tau_c \qquad (3.1)$$

where N_i is the density of cluster ions proportional to I_i, N_0 is the density of neutral clusters ejected through the nozzle, $\Omega(E_b)$ is the cross section for ionization, n_b is the density of electrons for ionization, E_b and V_b are the mean energy and the mean velocity of the electrons for ionization, and τ_c is the lifetime of cluster ions. Figure 3.10 shows the relation between I_i and V_a with constant I_e = 100 mA, and V_e = 200 V.

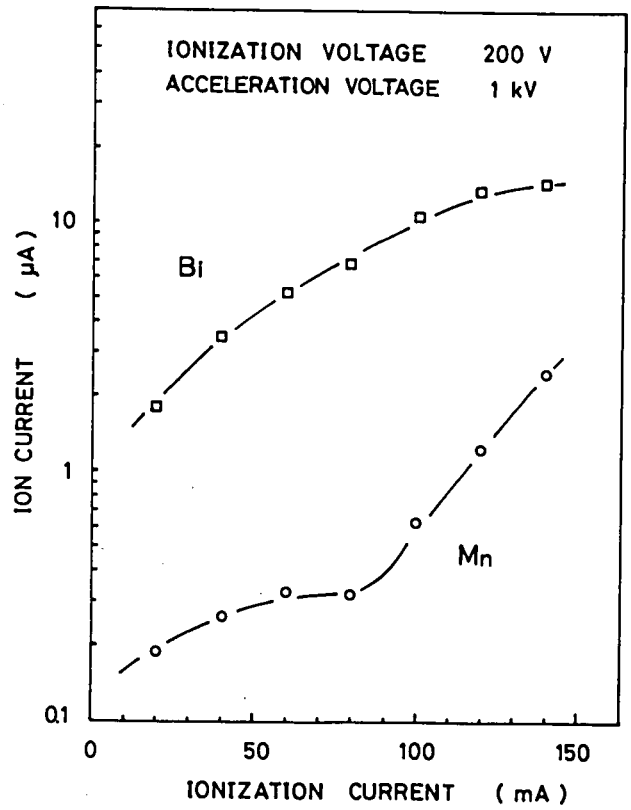

Fig. 3.9 Dependence of the ion current I_i on the electron current for ionization I_e.

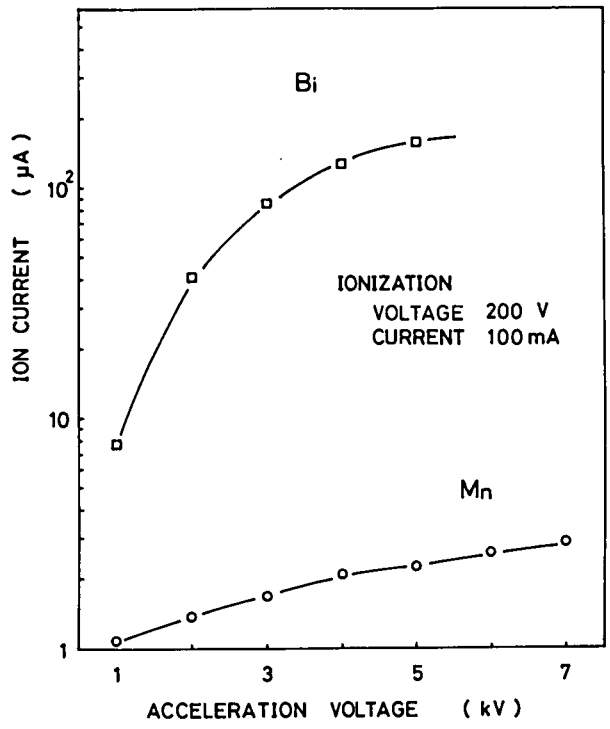

Fig. 3.10 Dependence of the ion current I_i on the acceleration voltage V_a.

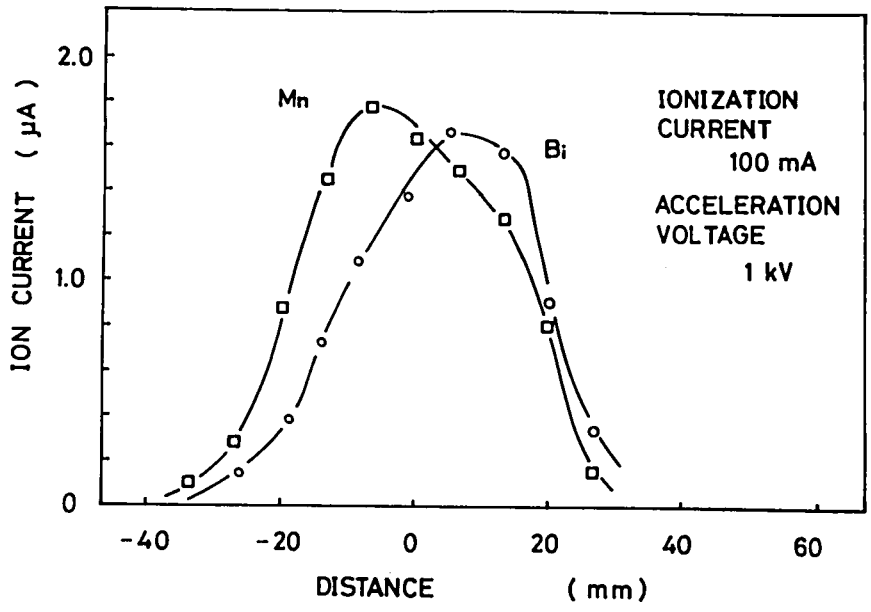

Fig. 3.11 The spatial distribution of the ion current I_i at the substrate.

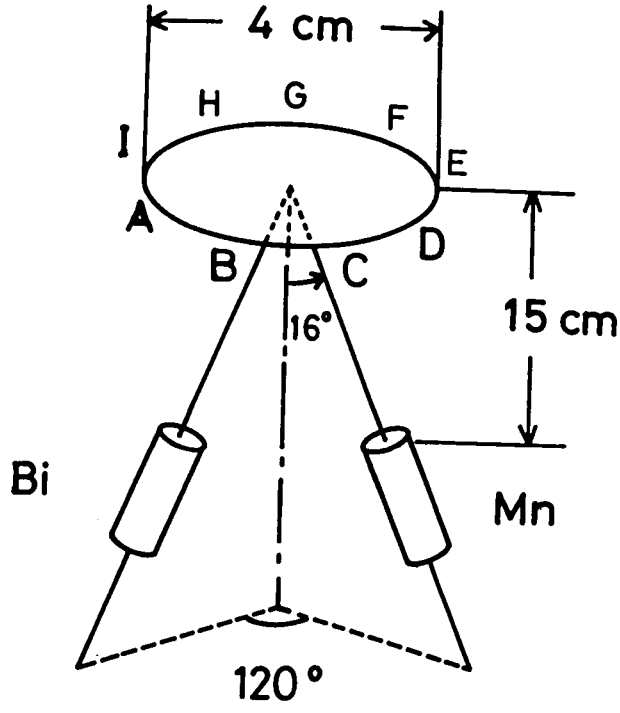

Fig. 3.12 The arrangement of crucibles and the substrate plane.

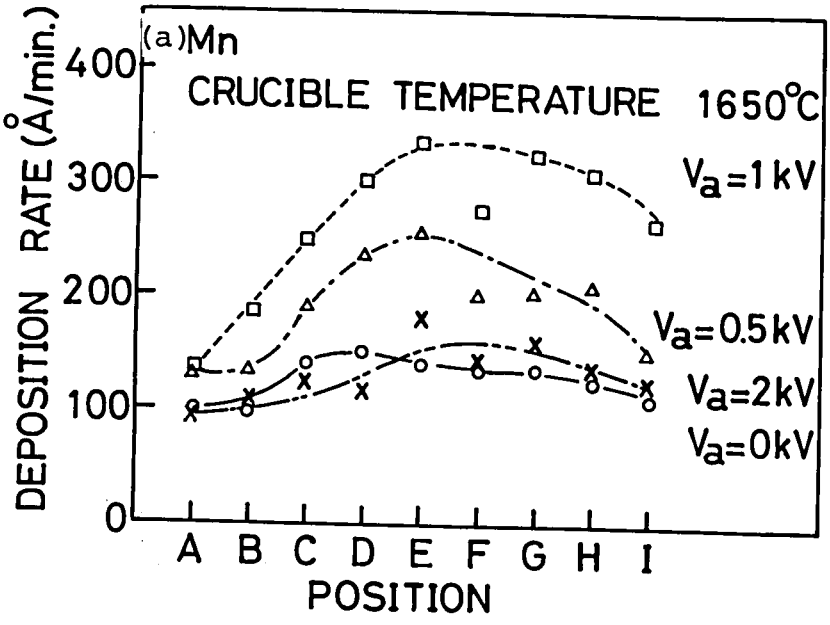

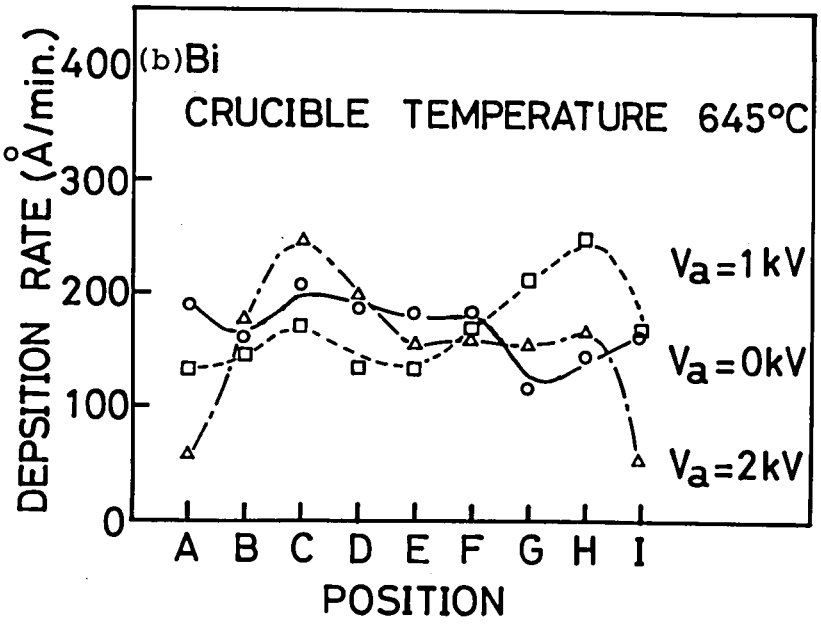

Fig. 3.13 The deposition rate of (a)Mn and (b)Bi at various position.

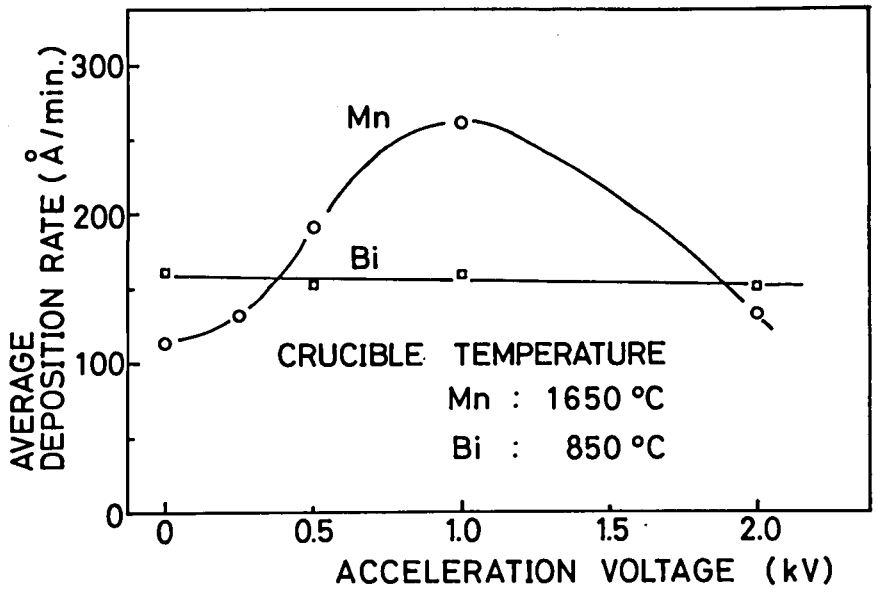

Fig. 3.14 The average deposition rates of Mn and Bi.

In a case of Mn clusters, I_i is proportional to $V_a^{1/2}$, while I_i of Bi clusters is saturated above V_a= 5 kV. The spatial distribution of I_i at the substrate measured by a current prove is shown in Fig. 3.11. The measured line was taken as the line between two intersections of the substrate plane and centers of two ICB source. The spatial distributions differ a little in center positions, but the total current is almost uniform in the area $\pm$ 3 cm.

Deposition rate of Mn and Bi were measured at the condition of V_e = 200 V, I_e = 100 mA and derived from deviding a film thickness by a deposition time. Film thicknesses were measured by a interferometer. The arrangement of Mn and Bi crucible and the notation of positions in substrate plane are illustrated in Figs. 3.12. In Figs. 3.13 (a) and (b), the deposition rate of each material was measured at the positions denoted in Fig. 3.12 taking V_a as a parameter. The average (positions from A to I) deposition rates deribed from Figs. 3.13 (a) and (b) were shown in Fig. 3.14. The deposition rate of Mn clusters exhibits the maxima around V_a = 1 kV, while those of Bi clusters is nealy constant. Taking account of the melting point of Bi as low as 271 °C, it is likely said that the reevaporation of Bi was taken place by the accelerated particles.

3.4 Summary

By using the ICB technique, thin films of intermetalic compounds are successfully obtained with good uniformity. Since the ICB technique is classified as one of the ion-based

technique, the deposition process in a high vacuum is basically stable and reliable. Reproducibility of the film formation and the stoichiometry of the film composition are achieved by controlling the deposition parameters. Moreover, the physical and crystallographical characteristics of the deposited films can be adjusted suitablly for the magnetooptical recording material by controlling these parameters according to the source material and the substrate.

IV MnBi FILMS

4.1 Introduction

4.1.1 Crystallographic Phases of MnBi

MnBi possesses two crystallographic phases: the low temperature phase (LTP) is ferromagnetic and has a NiAs structure, as illustrated in Fig. 4.1, with a Curie temperature of 360°C [65]. Beyond this temperature a first order transition take place with some of the Mn atoms occupying interstitial site (trigonal bipyramidal hole with coordination number 5) [66], resulting in the high temperature phase (HTP) which has a distorted NiAs structure of orthorhombic system. The amount of the interstitial Mn atoms are estimated as 9.9 % by B.W.Roberts[67] and 15 % by A.F.Andressen[68]. If the medium is then properly quenched, this HTP can be retained at room temperature. This quenched high temperature phase (QHTP) is also ferromagnetic with a Curie temperature of 180 °C.

4.1.2 Magnetic properties

The temperature dependence of the magnetization has measured for both the LTP and the QHTP MnBi films by D.Chen et al. [65], as shown in Fig. 4.2. The saturation magnetization $4\pi M_s$ of LTP and QHTP MnBi films at room temperature were obtained as 7.2×10^3 and 5.5×10^3 (Gauss), respectively. The magnetic easy axis of MnBi aligns in parallel with the c-axis, and the uniaxial anisotropy constant K_u is estimated to be 11.2×10^6 (erg/cm^3) at room temperature [69]. Moreover, it is observed

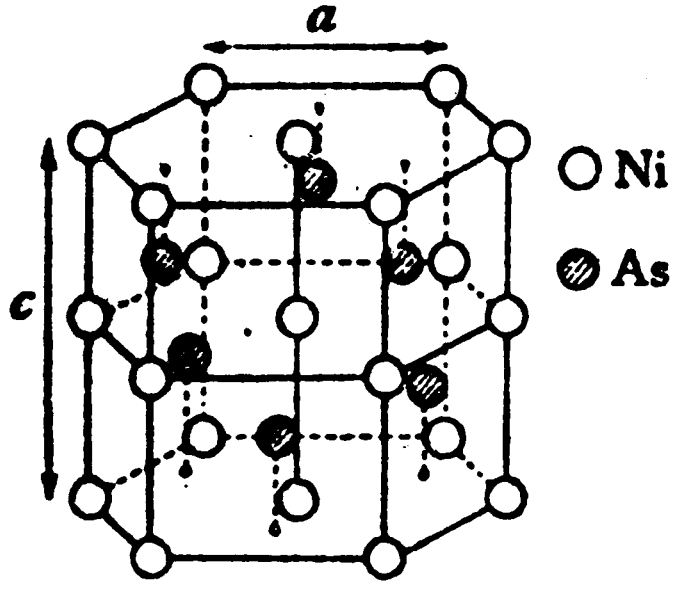

Fig. 4.1 Crystal structure of a NiAs type.

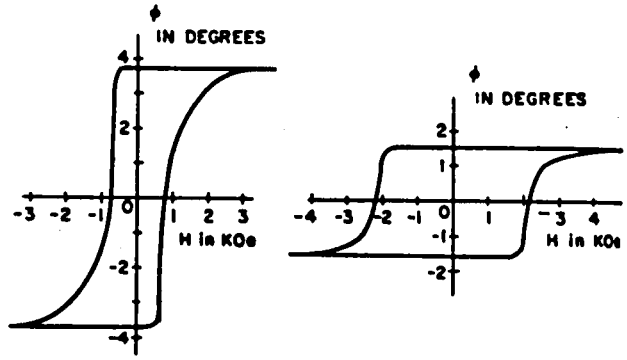

(a) LTP (b) QHTP

Fig. 4.2 The temperature dependence of the magnetization of the LTP and the QHTP MnBi films.

Table 4.1 The magnetic and crystallographic properties of the LTP and QHTP MnBi films.

	LTP			QHTP	
Crystallographic Stracture	NiAs			DISTORTED NiAs	
c_o (A°)	6.126	6.116	6.086	5.97	14.8
a_o (A°)	4.290	4.286		4.34	11.8
b_o (A°)	-	-	-	-	8.7
Curie Temperature(°C)	360			180	
Fig. of merit at 6328 A° (deg.)	3.0 ~ 3.6			1.4 ~ 1.6	
$4\pi M_s$ (Gauss)	7200			5500	
Coercivity (kOe)	0.75 ~ 2			2 ~ 4	
Field to Saturation (kOe)	3 ~ 4			4 ~ 6	
Magnetic Moment per Mn atom (μ_B)	4	3.84±0.03		1.17	3.07±0.04

that the anisotropy constant of MnBi between room temperature and 360 °C remains approximately constant. The coercivity H_c and the magnetic field to saturation which characterize the magnetic hysteresis of MnBi films were also obtained by several authors [70)-72)].

These magnetic as well as crystallographic properties of the LTP and the QHTP MnBi films are given in Table 4.1.

4.1.3 Historical Background in the Study of MnBi Films

A MnBi thin film was first prepared by H.J.Williams et al. by using a conventional vacuum evaporation in 1957 [74)]. The method of film preparation reported by Williams et al. is as follows: A layer of manganese and then a layer of bismuth are deposited sequentially on a glass substrate. This composit film is sealded off in a Pyrex tube and annealed at temperatures ranging from 225 to 350 °C for three days. Films prepared in this manner were not uniform and continuous, although the c-axis as well as the magnetization were perpendicular to the film surface. They also proposed the recording method that the writing process was done by a magnetic needle and the reading process by the Faraday effect. L.Mayer has studied the nucleation process in films by Williams' method, and carried out the Curie point writing on MnBi films by a hot needle and a electron beam [29),75)]. However, it was concluded that nucleation of MnBi starts on random sites, resulting in film growth being uncontrollable and a long annealing time being required.

With development of optical technology, especially with

the advance in laser technology, the magnetooptical recording was proposed by D.O.Smith in 1967 [76]. Laser beam is addressed on the memory system, and then used as a heat source in the writing process. The reading process is accomplished by either transmission or reflection of the same laser beam. With a pulsed He-Ne laser beam, D.Chen et al.[1] have made Curie point writing on MnBi films prepared by a modification of the Williams method. The major difference between them lies in the fact that the bismuth layer was deposited prior to the deposition of the manganese layer, and the annealing time was reduced considerably from a few days to a few minutes or a few hours. Subsequently, many studies have been reported for the memory application of a high density. The studies deal with the writing mechanisms[77], the magnetization within a written bit[3], the relation between a shape of a written bit and the film thickness[4], the techniques of a writing or erasing processes[2),5),78], modifications of preparing methods[6),7),79], domain nucleation processes[6),7),80)-83], magnetizing processes[71),83], the structure of magnetic domains[83),84], and the thickness dependency of coercivity and demagnetizing field[4),73] etc. At present, however, the films prepared using the conventional vacuum evaporation involve many problems to be solved, especially from viewpoint of a film uniformity over a large area and a stability in read, write, and erase over an essentially number of cycles. Uniform films of large area are difficult, if not possible, to be prepared by the method mentioned above, in which the double layer of manganese and bismuth, in principle, are

annealed so that the nucleation of MnBi crystallite is not precisely known to us. Moreover, the reproducibility of a film formation could not achieved yet, which was pointed out by Mayer [85] and G.Lewicki et al.[82] In addition, the adhesion strength between a film and a substrate is a important characteristic when the phase transformation LTP⇄QHTP causes the strain of a film in the writing process and the phase transformation LTP QHTP of a written bit seriously limit the reliability of MnBi films for memory storage planes, although this transformation does not affect information stored in the films. The transformation of LTP to QHTP is quite rapid. The reverse transformation is slower; a time constant ∿2 years at room temperature has been estimated [65]. This is too short for a practical memory system.

4.2 Film Preparation

Film preparation of MnBi by the ICB technique was made by the deposition of the accelerated Mn and Bi clusters onto a glass substrate. The source materials of Mn and Bi are mounted in separate crucibles, and they are heated at 1620 °C and 880 °C, respectively, to obtain a stoichiometric composition.

In this experiment, the Mn and Bi composite films are deposited simultaneously under the condition of electron current I_e for ionization 40-100 mA with no additional acceleration voltage of ionized clusters. It should be noted that even the neutral clusters have their kinetic energy of about 120 eV corresponding to their ejection velocity [61]. A silicon monooxide protection

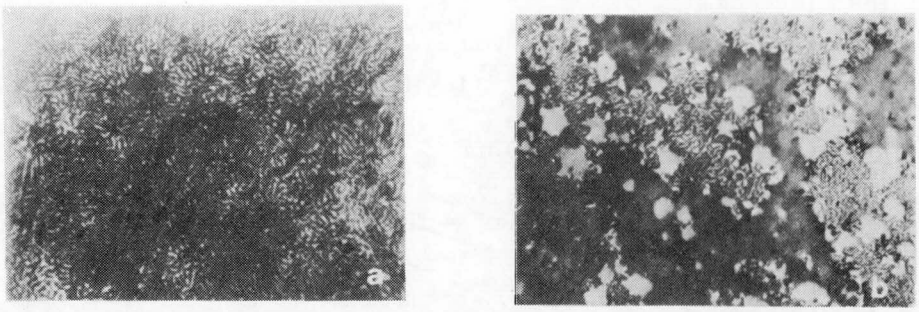

Fig. 4.3 Magnetic domain configurations of MnBi films prepared by (a)the ICB technique and (b)the conventional vacuum deposition.

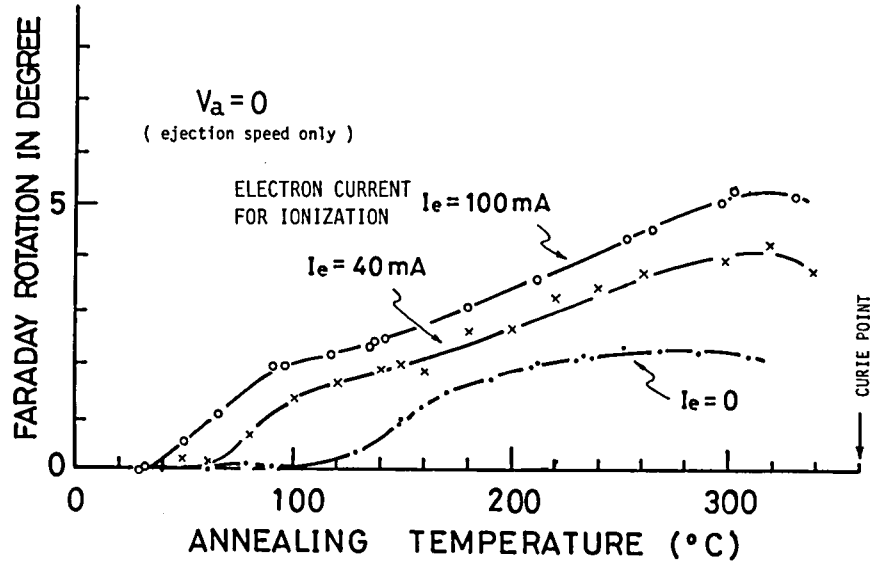

Fig. 4.4 MnBi growing process during annealing measured by magnetooptical Faraday effect.

layer is coated by the evaporation. The annealing temperature is up to the Curie point (360 °C) for a few minutes to a few hours.

4.3 Evaluations of MnBi Films

4.3.1 Crystallographic and Magnetic Properties

Studies have been made of magnetic domain configurations of thin MnBi films annealed under various conditions. Observation of domain patterns were achieved with a polarizing microscope with reflecting light by employing the Kerr effect. In Figs. 4.3 (a) and (b), a typical magnetic domain structure of MnBi film deposited simultaneously with Mn and Bi by the ICB technique onto a glass substrate, followed by annealing at 300 °C for 3 hr., is compared with that of the film deposited simultaneously by the conventional vapour evaporation without ions. The deposition conditions in the ICB technique were I_e(electron current for ionization)= 100mA and V_a(acceleration voltage)=0, and the vacuum during deposition is in the range 10^{-6}-10^{-5} Torr. As seen in Fig. 4.3(a), uniaxial stripe domain with perpendicular easy to the film surface appear all over the glass substrate (5 x 5 cm^2). On the contrary, for the simultaneous method of conventional vacuum evaporation as shown in Fig. 4.3(b), the domain configurations of an islands-like structure grew, and the remaining part of non magnetic materials such as manganese oxides and bismuth oxides. A sequential method of film preparation, that is, the deposition of the bismuth layer prior to the manganese layer, was carried out, but the uniformity over

the large area also could not be obtained.

To investigate the crystallographic and magnetic domain growth of MnBi films, measurements of the Faraday rotation at the He-Ne laser wavelength 6328 Å and X-ray diffraction were made with respect to composite films of the thickness 500 Å, which are deposited at I_e= 0, 40 and 100 mA keeping V_a= 0, that is, with only the kinetic energy corresponding to the ejection velocity of clusters. In the measurements of the Faraday rotation, the films were magnetically saturated by applying a magnetic field at 6 kOe in a direction perpendicular to the film surface. Figure 4.4 shows the change of the Faraday rotation as a function of temperature at a rising rate of 10 °C/min. The Faraday rotation which suggests the growth of a ferromagnetic MnBi can be observed at temperature below 80 °C. The annealing of films at elevated temperature from 80 °C to 300 °C is found to increase the Faraday rotation, and in this region a pronounced increase in the rotation angle can be seen at higher amount of ionized clusters. On the other hand, by using a conventional method where the double layer were deposited on mica substrate, the Faraday rotation arises at around 220 °C [65]. Below 220 °C, the Faraday rotation could not be observed. There are distinct difference with regard to the magnetic domain growth process between the ICB technique and the conventional method. This result lead us to believe that the presence of ions and the kinetic energy of clusters toward the substrate produce the marked change in the critical condensation

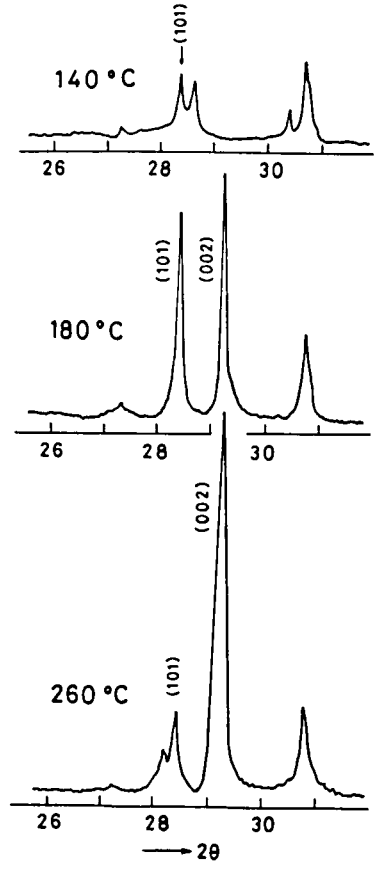

Fig. 4.5 X-ray diffraction patterns of MnBi films as a function of the annealing temperatures, 140, 180 and 260 °C, respectively.

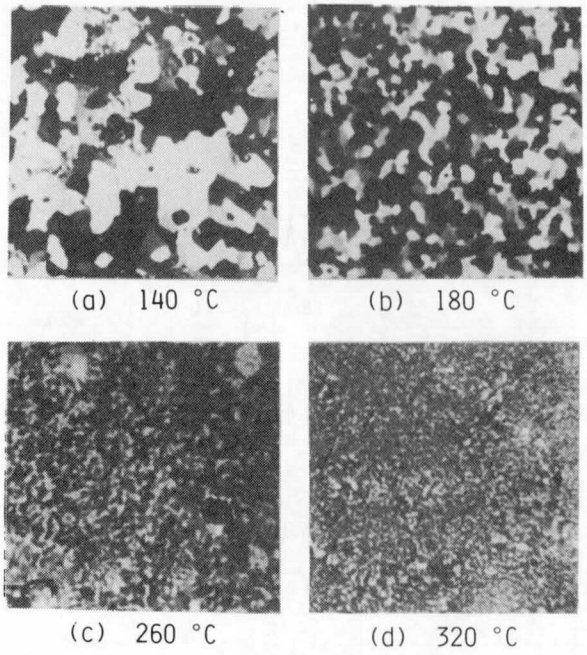

Fig. 4.6 Magnetic domain configurations of MnBi films annealed at different tempeatures.

pressure of the source materials, which is closely related to the nucleation and growth mechanism of the films.

Futher details on the film growth mechanism, especially in the range 100 °C to 300 °C, could be obtained from measurements of the X-ray diffraction and the polar Kerr effect. The X-ray diffraction patterns of the films, which were air-quenched at a rate of 3 °C/min from different temperatures, are shown in Fig. 4.5. It is observed that crystal growth having a (101) plane of MnBi takes place at 140 °C; however, a rapid formation of a (002) plane corresponding to the c-axis of this material takes place near 180 °C together with the marked (101) plane. Preferential orientation to the c-axis, 002 , is seen to enhance itself remarkably when the annealing temperature is about 260 °C. Typical domain patterns observed by the polar Kerr effect are shown in Fig. 4.6, from which it was found that the large scale magnetic domains are formed at comparatively low annealing temperature (e.g. 140 °C), and that uniaxial fine domains appear with annealing at elevated temperature as high as 180 °C. Since the magnetic easy axis of MnBi films align in parallel with the c-axis and perpendicular to the substrate surface, the appearance of the uniaxial and fine magnetic domains suggests that the crystal growth with a preferential orientation to the c-axis takes place at least above 180 °C, which is consistent with the result of the X-ray diffraction measurement.

In order to investigate the degree of preferential orien-

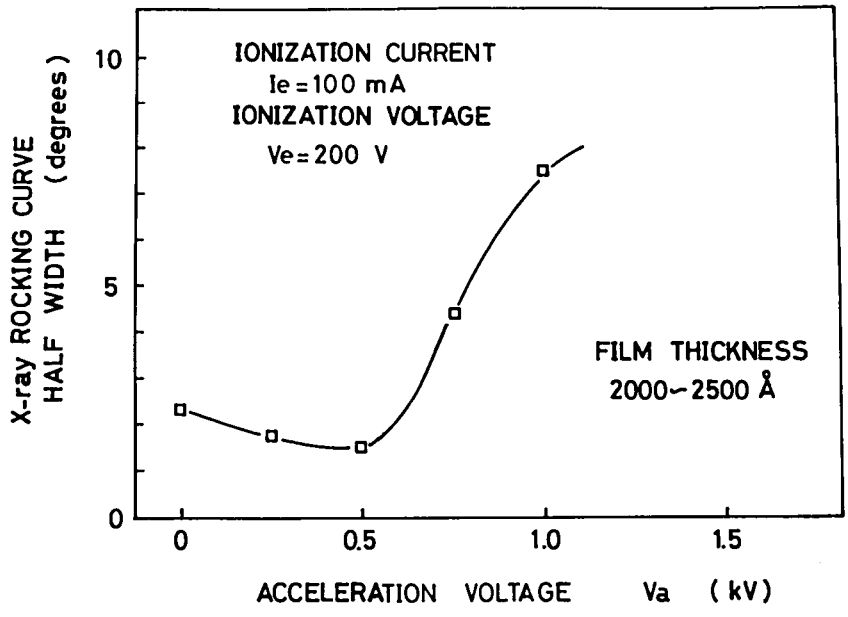

Fig. 4.7 The half width of MnBi(002) rocking curves as a function of the acceleration voltage V_a.

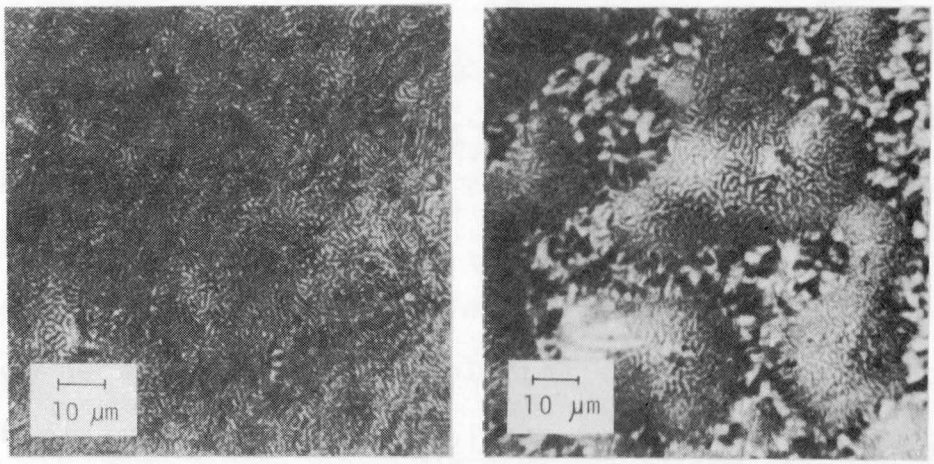

Fig. 4.8 Magnetic domain configurations of MnBi films deposited at (a)V_a= 0 and (b)V_a= 4 kV.

tation, that is, the variation of c-axis direction, X-ray rocking curves were measured as a function of the acceleration voltage V_a for the films annealed at 300 °c, 2 hr. Figure 4.7 shows the half width of MnBi(002) rocking curve in which the spreading of incident X-ray is not taken into consideration. It is observed that the half width is gradually decreases with increasing V_a from 0 to 0.5 kV, and extremely increases with increasing V_a more than 0.5 kV. This increasing of the half width of X-ray rocking curve coincides with the magnetic domain configuration, as shown in Fig. 4.8. When V_a= 0(Fig.4.8(a)), uniform stripe domains appear all over the substrate surface, while the stripe domains form locally in many places for V_a= 4 kV(Fig. 4.8(b)). The difference in these magnetic domain configurations as well as X-ray rocking curves may be due to the fact that the orientation to the c-axis is weaker during deposition because of sputtering effects and migration effects of the accelerated ionized clusters on the substrate. Although the stripe domain develop locally for V_a= 4 kV, they extend without any restrictions on crystal growth from the middle of MnBi nuclei, whereas similar stripe domain in films formed by the conventional technique have only been observed in single-crystal platelets of MnBi compounds [86].

Since the spreading of incident X-ray is estimated to be an order of one or two degree, it is said that only ejection velocity (V_a=0) is sufficient to obtain a c-axis preferentially oriented film on a glass substrate for MnBi films by the ICB technique.

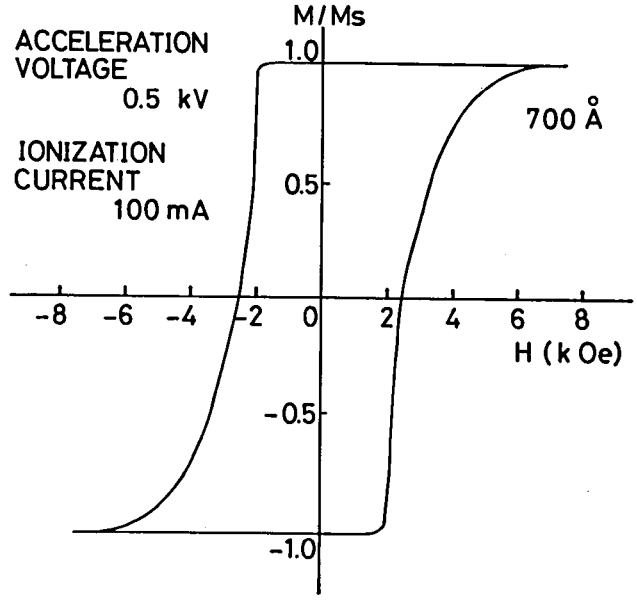

Fig. 4.9 The typical magnetic hysteresis of a MnBi film by using the Faraday effect.

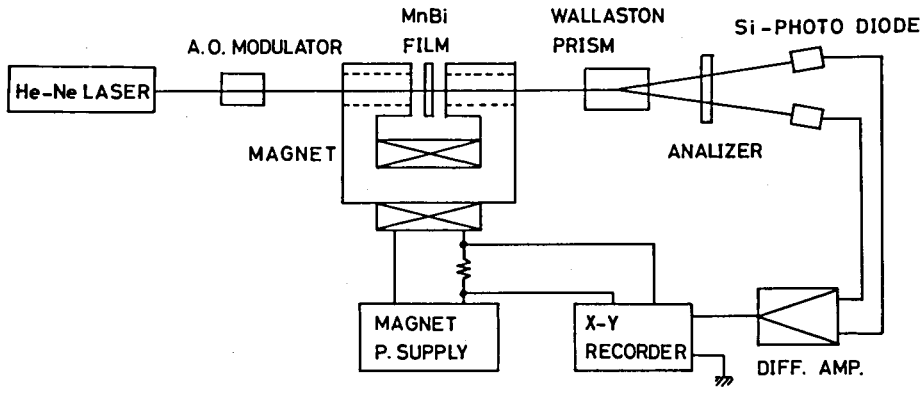

Fig. 4.10 The block diagram of the experimental setup for measuring the magnetic hysteresis by using the Faraday effect.

Figure 4.9 shows a typical magnetic hysteresis obtained by using the Faraday effect. The schematic diagram of the measuring system is shown in Fig. 4.10. The film having a rectangular hysteresis is considered to be suitable for a magneto-optical memory material, as mentioned in Chapter II.

4.3.2 Optical Properties

Since optical properties are very important for a magneto-optical recording material as previously discussed in Chapter II, the optical properties of MnBi films are investigated with an optical absorption coefficient α and the specific Faraday rotation as a function of wavelength and the Kerr rotation. The specific Faraday rotation is defined as the Faraday rotation in degrees per cm. The reflectivity and the transmisivity of a MnBi film were measured by a spectrometer (Shimazu, MPS-50L) at wavelength ranging from 400 nm to 2000 nm, as shown in Fig. 4.11, where R_G and R_s are reflectivities of a glass substrate side and a SiO protective layer side, respectively, I_T/I_0 the transmisivity of the film. The absorption in a short wavelength is caused by the absorption of free electron [65].

For determining the absorption coefficient, the correction for the reflection at each interfaces were made as follows: [87] Since the absorption loss is large in the magnetic layer, the multiply reflected light in the magnetic layer is neglected. First, the reflectivity R_M in the interface between the magnetic layer and the substrate is given by

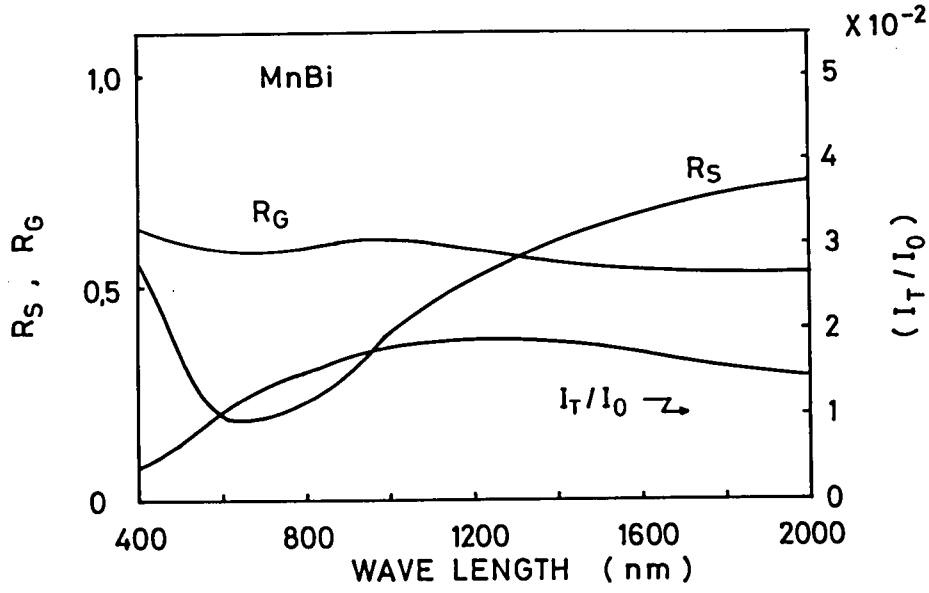

Fig. 4.11 The reflectivity and the transmissivity of the MnBi film.

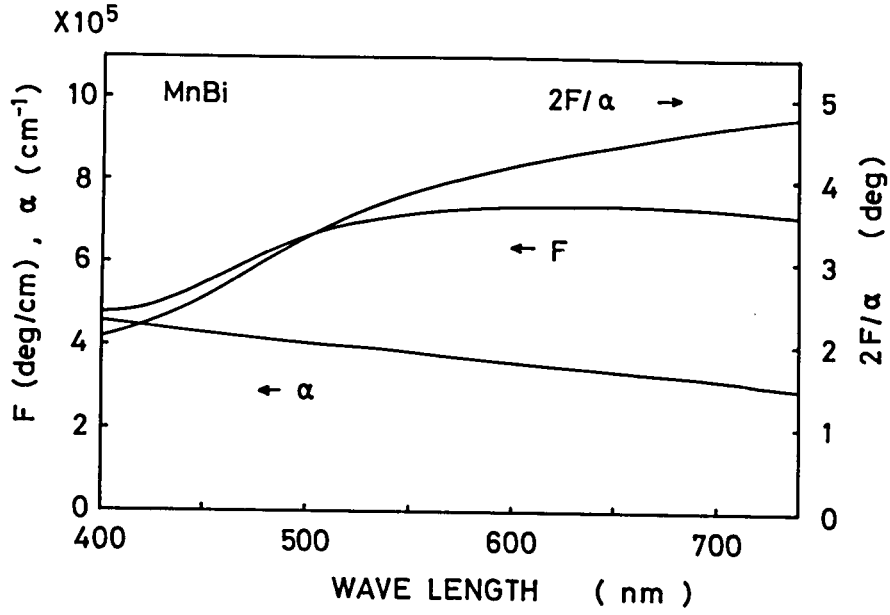

Fig. 4.12 The optical absorption coefficient α, the specific Faraday rotation F and the figure of merit $2F/\alpha$ of the MnBi film.

$$R_G = R' + (1-R')^2 R_M \ , \qquad (4.1)$$

where R' is the reflectivity at the substrate-air interface which is defined as

$$R' = \left| \frac{1+n_s}{1-n_s} \right|^2 , \qquad (4.2)$$

where n_s is the refractive index of the substrate material. Since n_s depends on wavelength, the reflectivity R' was measured practically in the same wavelength range as above.

Then the absorption coefficient α is determined by

$$I_T/I_0 = (1-R')(1-R_M)(1-R_s)e^{-\alpha t} \ , \qquad (4.3)$$

that is

$$\alpha = -\frac{1}{t}[\ln(I_T/I_0) - \ln(1-R_M) - \ln(1-R_s) - \ln(1-R')] , \qquad (4.4)$$

where t is the film thickness. The result is shown in Fig. 4.12.

The Faraday rotation is measured as a function of wavelength. Figure 4.13 shows a block diagram of the experimental setup. The film is magnetically saturated to a direction by applying external magnetic field (10 kOe) perpendicular to the film surface in advance, and the analyser angle is measured as θ_1 when the output of the photo mutiplier (P.M.) is minimum. Then the film is placed in the opposite direction and the

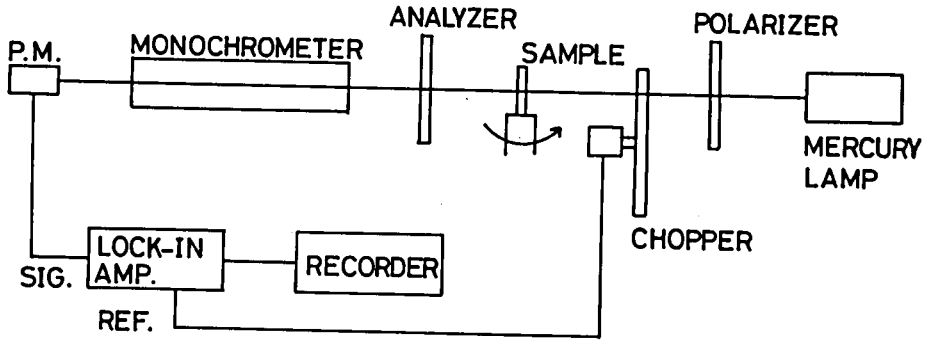

Fig. 4.13 The block diagram of the experimental setup for measuring the Faraday rotation.

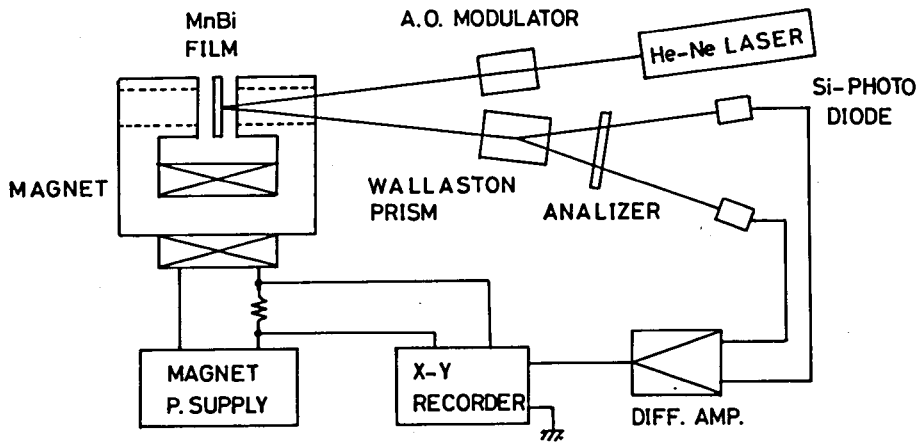

Fig. 4.14 The block diagram of the experimental setup for measuring the Kerr rotation.

analyser angle θ_2 is obtained as in the same manner. The total Faraday rotation F_t is determined as

$$F_t = \frac{1}{2}|\theta_1 - \theta_2| \ , \qquad (4.5)$$

and the specific Faraday rotation F is obtained by deviding F_t with the film thickness. The result is shown in Fig. 4.12. The figure of merit $2F/\alpha$ is also shown in the same figure by using the absorption coefficient α obtained from Eq.(4.4). At 6328 Å the specific Faraday rotation F and the figure of merit $2F/\alpha$ were obtained to be 7.4×10^5 deg/cm and 4.5 deg., respectively. Comparing with reported values $F = 7.3 \sim 7.6 \times 10^5$ deg/cm [65),79)] and $2F/\alpha = 2.85 \sim 2.6$ deg. [1),65)], the absorption coefficient α is found to be small resulting in a half as large as the value of the figure of merit $2F/\alpha$.

The Kerr rotation was measured with the experimental setup shown in Fig. 4.14. The obtained values from the SiO layer side and the substrate side were 2.0 and 1.5 deg., respectively. The larger value of the SiO layer side is interpreted by the fact that the Kerr rotation is enhanced by the overcoated dielectrics with n_1 times, where n_1 is the refractive index of the dielectrics. For a SiO layer, the enhancement of the Kerr rotation is about 5 times at the maximum [89)].

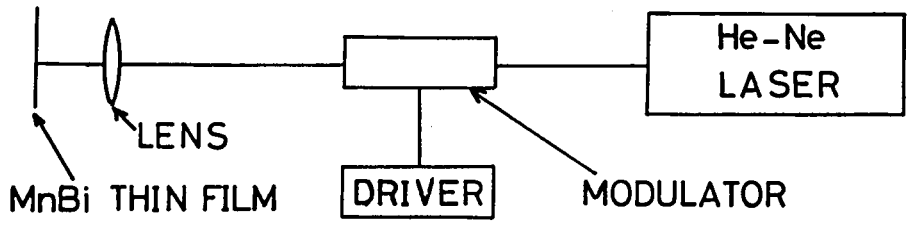

Fig. 4.15 The block diagram of the experimental setup for Curie point writing.

4.4 Curie Point Writing in MnBi Films

4.4.1 Apparatus

Figure 4.15 shows a block diagram of the experimental setup of Curie point writing in the MnBi films. The He-Ne laser with the maximum power 50 mW at 6328 Å in wavelength (Kinmon electric Co. Ltd., KLG-103), the acoustooptical (A.O.) modulator (ISOMET, 1201C-1), and objective lenses (numerical aperture 0.25 and 0.4) for forcusing the laser beam were used for this experiments. Figure 4.16 shows the laser and the modulator, figure 4.17 the forcussing lens and the film.

The films used in this experiment were deposited with V_a = 0, thickness 1000 Å, and overcoated with a SiO layer of 1000 Å. And they were cooled down from above the Curie temperature to a room temperature with a cooling speed of 3 °C/min in a magnetic field perpendicular to the film surface of 8 kOe in order to the magnetization of a MnBi film being aligned to one direction with the intension of using the demagnetizing field and no additional magnetic field in writing. The A.O. modulator can be operated with a positive logic of the TTL level so that the pulse width of the laser beam is controlled by a one-shot multivibrator whose circuits is shown in Fig. 4.18. The written domain were observed under a polarising microscope using the Kerr effect.

4.4.2 Experimental Results

Figure 4.19 shows the written domains of cicular spots and a line configuration with the objective lens of N.A. 0.25.

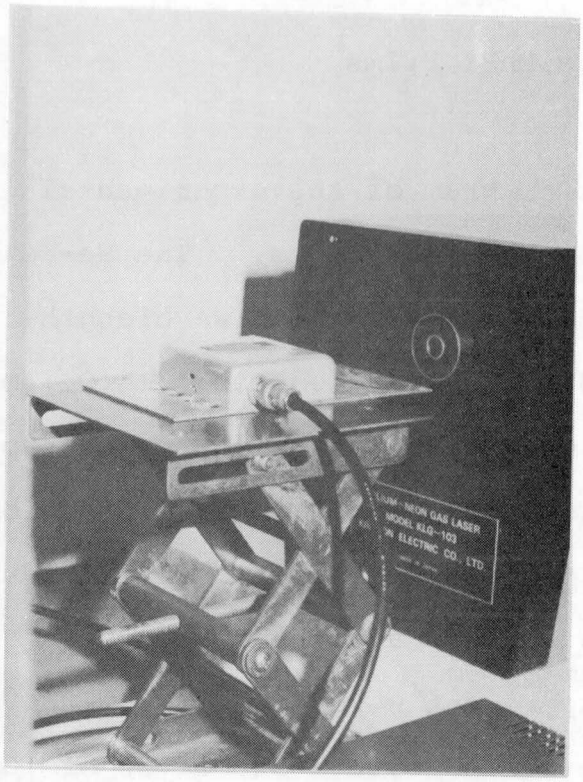

Fig. 4.16 The view of the He-Ne laser and the acousto-optical modulator.

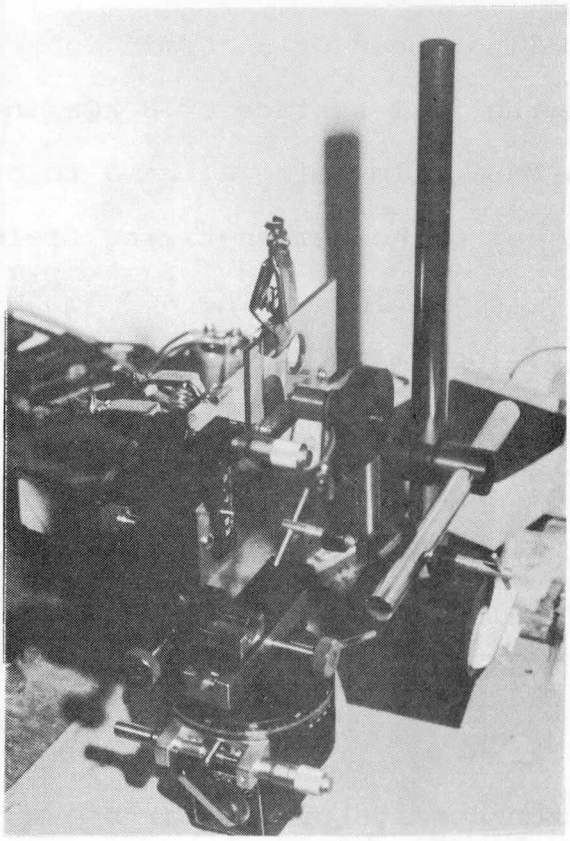

Fig. 4.17 The view of the forcussing lens and the film holder.

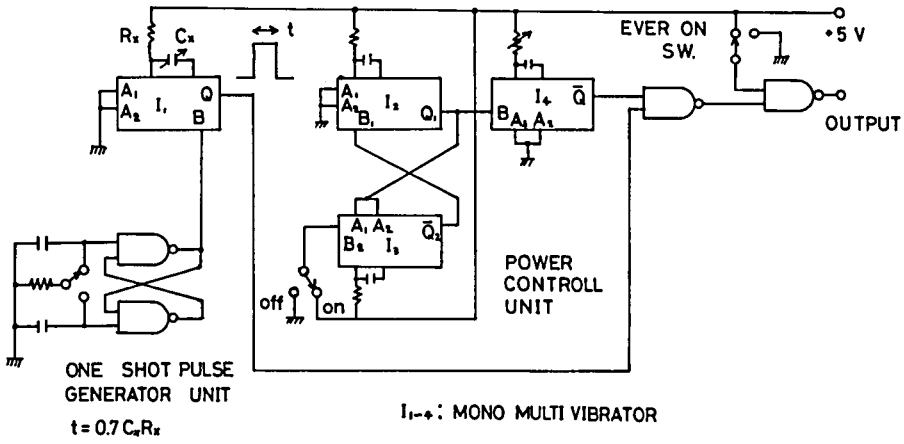

Fig. 4.18 The circuit diagram of the one-shot multivibrator.

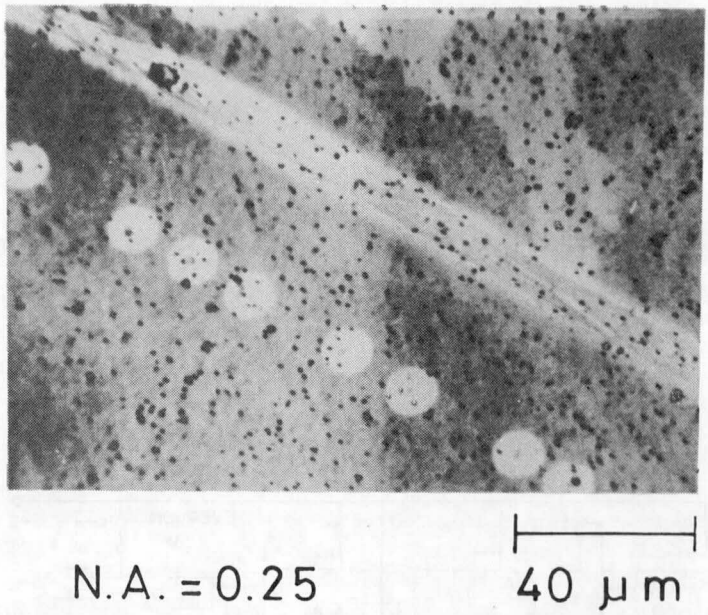

Fig. 4.19 The view of written domains with the objective lens of N.A. 0.25, observed under polarizing microscope.

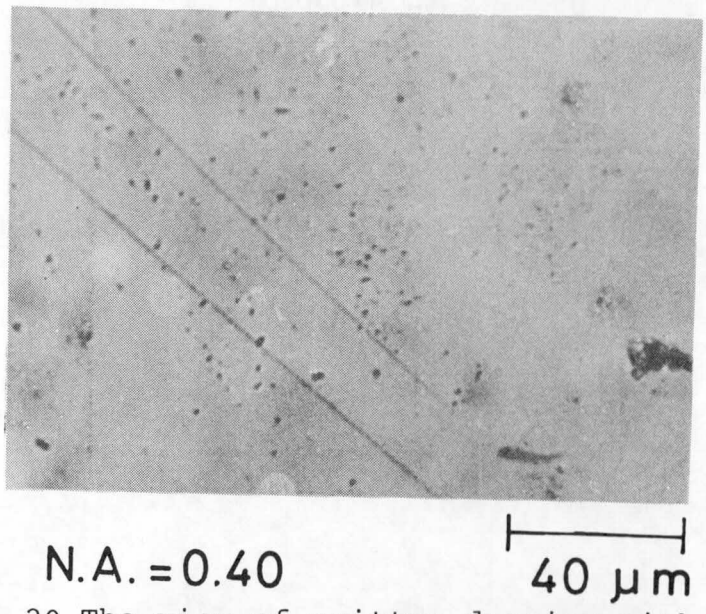

Fig. 4.20 The view of written domains with the objective lens of N.A. 0.4, observed under polarizing microscope.

Circular spots were written with a laser power 50 mW,light pulse width 1 msec, and whose diameter was about 9 μm. The line shape domain was written with a laser power 50 mW,scanning speed of the laser beam ∿3 cm/sec, and whose line width was about 10.5 μm. The inside of the line shape domain is demagnetized because the cooling process starts from the edges of a Gausian laser beam so that the demagnetizing field acting on the area just below the Curie temperature changes its direction alternately. Figure 4.20 shows line shape domains written at the same condition with the objective lens of N.A. 0.4. The line width is found to be less than 1.5 μm and is not demagnetized within the line. There exist the interdependence between the laser power and the light pulse width. Figure 4.21 shows the area of written spots as a function of the beam power and the pulse width by using the objective lens of N.A. 0.25. The ranges of the laser power and the pulse width are greater by one order as compared with the reported values by Lewicki et al. [90] because of the difference in the film thickness and the optical absorption coefficient α. The film thickness is large and the optical absorption coefficient α is small as compared with the results of Lewicki et al., resulting in the large power and pulse width requirements in this experiment. The diameter of written spots as a function of the pulse width is shown in Fig. 4.22 with the laser power 50 mW and the objective lens of N.A. 0.25. By expolating the curve to the zero diameter, we can obtain the minimum pulse width as 400 μsec. This is also greater by one order than Lewicki's results

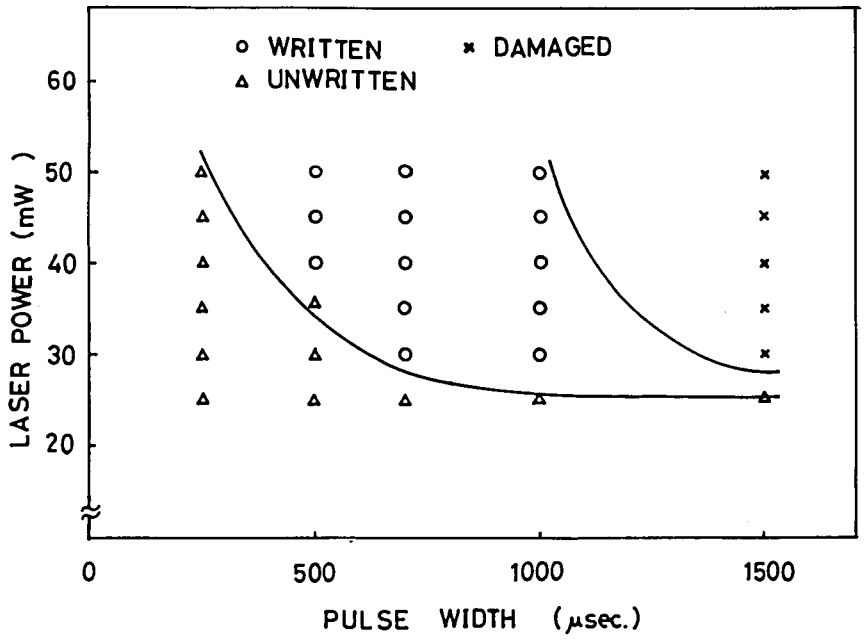

Fig. 4.21 Area if written spot as a function of the beam power.

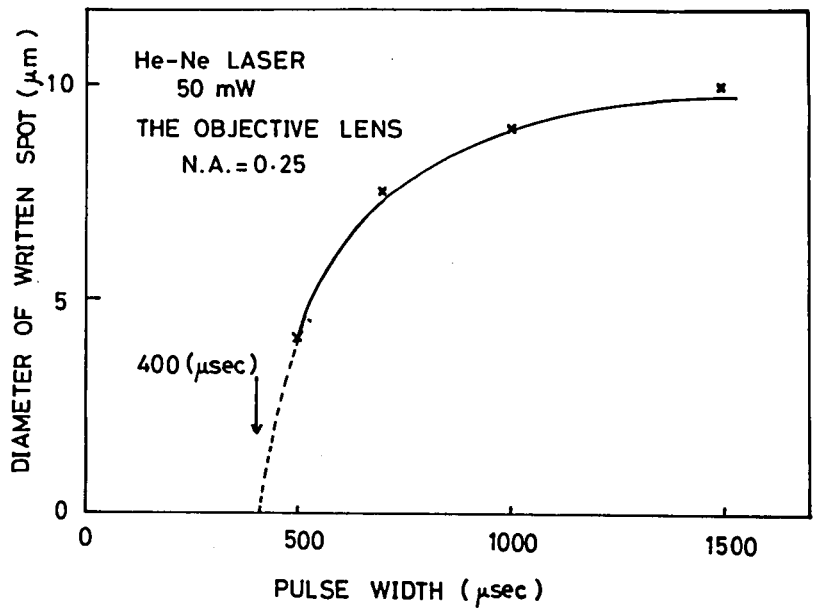

Fig. 4.22 The diameter of written spots as a function of the pulse width.

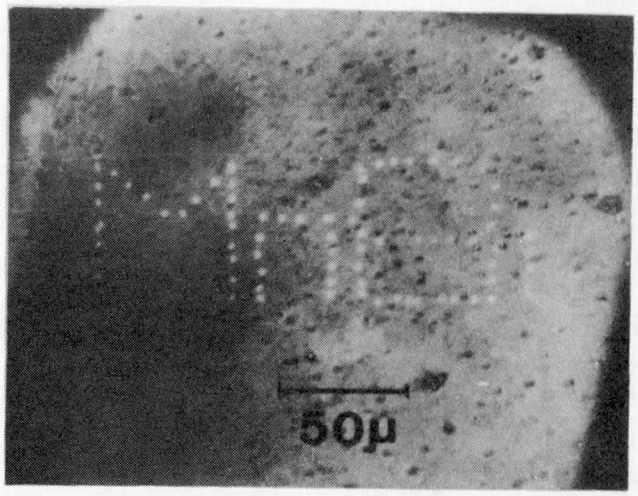

Fig. 4.23 An example of patterns written on MnBi films with thickness 1000 Å by He-Ne laser (wavelength 6328 Å, mW).

because of the fact mentioned above.

Figure 4.23 shows the spot patterns written on MnBi thin film, whose thickness is about 1000 Å, with a numerical aperture up to 0.25, and with the access time 10 msec. The bright spots (each diameter is 2 μm) are placed at intervals of 5 μm, resulting in the recording density of about 4×10^6 bit/cm^2. High stability of the film after writing and erasing over a substantial number of cycles was maintained, which proves that the adhesion strength of the film on the substrate is prominent. In order to get some information about the crystallographic structure of the written part of the film, X-ray diffraction pattern was measured. Figure 4.24 shows the results (a) before and (b) after writing. The crystal structure was found to change from LTP to QHTP by writing.

4.4.3 Observation of a Fourier Power Spectrum

In a case of the utilization of MnBi films for magnetic holographic storage, the many advantages based on the coherent optical system such as redundancies against scratches, dust or positioning of the film can be expected. In this section, the Fourier power spectrum which is concerned with the Fourier transformation type holography is observed. Figure 4.25 shows the arrangement of the experimental setup. The MnBi film and a screen are placed at a distance of the focal length of the lens (15 cm in this experiment) in order to make the Fourier transformation of the written domain in the MnBi film. Figure 4.26 shows the result obtained from the line shape domain whose

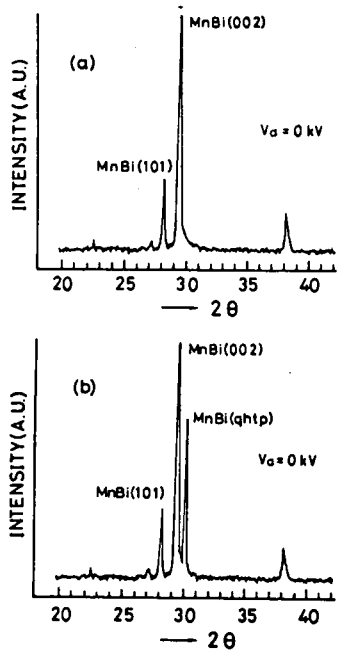

Fig. 4.24 X-ray diffraction patterns of MnBi films (a) before and (b) after writing by He-Ne laser.

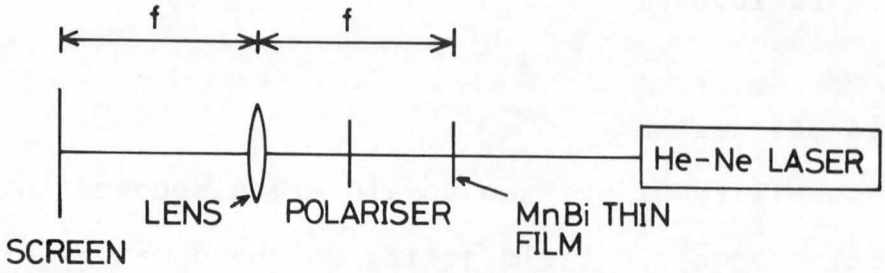

Fig. 4.25 The arrangement of the experimental set-up for observation of the Fourier power spectrum.

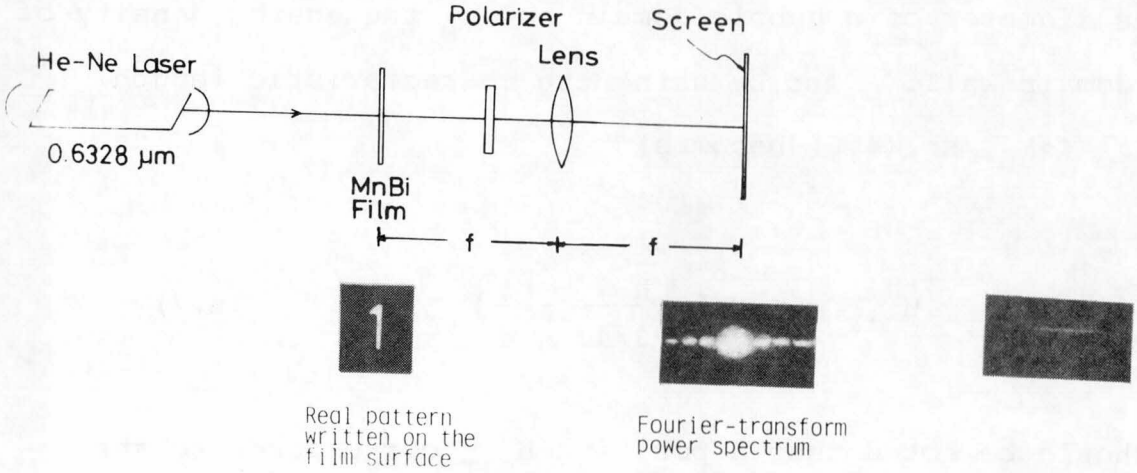

Fig. 4.26 The Fourier power spectrum obtained from a line shape domain.

line width is 10.0 μm.

4.4.4 Discussion

The stability of written domain are discussed in terms of the effective magnetic field acting on the domains. For a circular shape domain, the effective magnetic field H_{cir} acting on it is given by the bubble domain theory [91], which is

$$H_{cir} = \frac{4\pi M_s h}{h+3/4d} - \frac{\sigma_w}{M_s d} \quad [Oe], \qquad (4.6)$$

where M_s is the saturation magnetization, h the film thickness, d the diameter of a bubble domain and σ_w the energy density of the domain wall. And by using the characteristic length $l = \sigma_w/4\pi M_s$, Eq.(4.6) becomes

$$H_{cir} = 4\pi M_s\left(\frac{h}{h+3/4d} - \frac{l}{d}\right) \quad [Oe]. \qquad (4.7)$$

It should be noted that a positive H_{cir} corresponds to the spreading force on the domain and a negative H_{cir} to the shrinking force on the domain. Since $l = 320$ Å [92] and $4\pi M_s = 7.2$ K Gauss in the MnBi film, the effective field H_{cir} is obtained as 79.5 Oe applying h = 1000 Å and d = 9 μm, as shown in Fig. 4.19. Judging from this value, the domain must be spread, but the real circular domain still exists. Although Eq.(4.7) is led supposing that the domain wall coercivity is negligible as

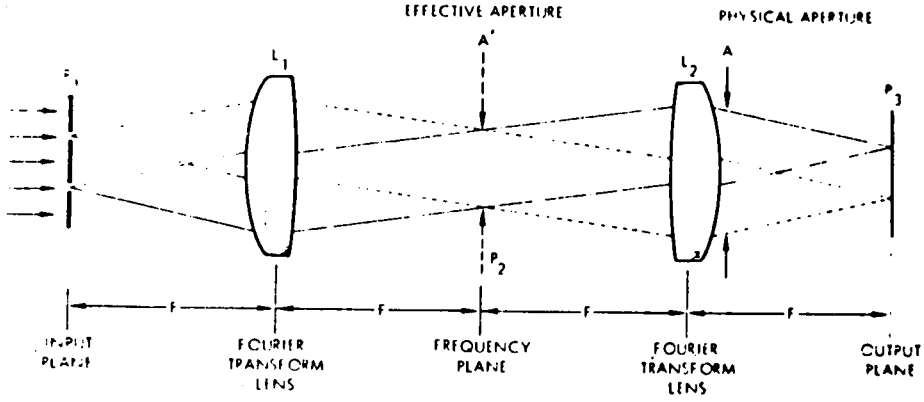

$$G(p,q)=\int_{-\infty}^{\infty}\int g(x,y)\exp\left[-j(px+qy)\right]dx\,dy$$

$$p=\frac{2\pi\xi}{\lambda F},\quad q=\frac{2\pi\eta}{\lambda F}$$

Fig. 4.27 Schematic diagram of the Fourier transformation system.

in a case of a single crystal material, MnBi films realy have the domain wall coercivity ranging from 0.75 to 2.0 kOe which is large enough to stabilize the domain against the effective field, and consequently the circular domains is found to be exist well by the domain wall coercivity. For a line shape domain, the spreading force in terms of magnetic field H_{line} due to the minimization of the magnetostatic energy is given by [93]

$$H_{line} = \frac{8\pi M_s}{\pi}\left[\tan^{-1}\left(\frac{h}{w}\right) - \frac{w}{2h}\ln\left(1+\frac{h^2}{w^2}\right)\right] \text{Oe}, \quad (4.8)$$

where w is the line width of a infinite line shape domain. Applying h = 1000 Å, $4\pi M_s$= 7.2 kOe, and w = 1.5 μm shown in Fig. 4.20 into Eq.(4.8), the spreading field could be estimated as H_{line}= 152.7 Oe. In this case, the domain wall coercivity also is found to play an important role for stabilizing the domain.

Following discussion deals with the Fourier power spectrum. In the Fourier transformation system as shown in Fig. 4.27, the complex amplitude of a light at (x,y) coordinates on the P_1 plane is noted as g(x,y) and that at (ξ,η) coordinates on the P_2 plane is noted as G(p,q) where $p=2\pi\xi/\lambda F$ and $q=2\pi\eta/\lambda F$, λ is the wavelength of a light, F the focal length of the lens L_1. The relation between g(x,y) and G(p,q) is given by [94]

$$G(p,q) = \int_{-\infty}^{\infty}\int g(x,y)\ \exp[-j(px+qy)]\ dxdy, \quad (4.9)$$

where j is the imaginary unit. Eq.(4.9) represents the Fourier transformation.

Considering with the Fourier transformation of a line shape domain as shown in Fig. 4.19, g(x,y) is then defined as

$$g(x,Y) = a \ , \quad |x| < x_0 \text{ and } |y| < y_0 \ , \qquad (4.10)$$

where x_0, y_0 and a are some constants and $y_0 >> x_0$ is settled. Consequently, G(p,q) is determined as

$$\begin{aligned} G(p,q) &= \int_{-y_0}^{y_0} \int_{-x_0}^{x_0} a \cdot e^{-jqy} \cdot e^{-jpx} dxdy \\ &= \frac{ax_0y_o}{4} \cdot \frac{\sin px_0}{px_0} \cdot \frac{\sin qy_0}{qy_0} \ , \end{aligned} \qquad (4.11)$$

The term $\sin qy_0/qy_0$ can be neglected because of the assumption $y_0 >> x_0$ so that Eq.(4.11) becomes

$$G(p,q) = \frac{ax_0y_0}{4} \cdot \frac{\sin px_0}{px_0} \ . \qquad (4.12)$$

The power of a light is defined as

$$|G(p,q)|^2 = A \cdot \left(\frac{\sin px_0}{px_0} \right)^2 \ , \qquad (4.13)$$

where $A = a^2x_0^2y_0^2/16$. Eq.(4.13) is in good agreement with the observed power spectrum as shown in Fig. 4.26 in which the light power becomes to zero alternatively and the peaks of

maxima decreases with the distance from the center spot. Since the period in Eq.(4.13) is px_0, the relation between x_0 and ξ_0 which mean the observed period (0.5 cm in the case of Fig. 4.26) is given by

$$x_0 = \frac{\lambda F}{2\xi_0} \quad . \tag{4.14}$$

Applying λ = 6328 Å, F = 15 cm, and ξ_0 = 0.5 cm into Eq.(4.14), x_0 could be estimated to be 9.5 μm which coincides with the value 10.0 μm observed directly under a polarizing microscope by using the Kerr effect.

4.5 Summary

The ICB deposition technique could be successfully applied to prepare large scale uniaxial thin films of MnBi suitable for thermomagnetic recording application. In the present study the films were easily prepared by a simultaneous method of the ICB deposition of Mn and Bi onto a glass substrate, and found to be extremely uniform over a large area and easily reproducible. The nucleation and crystal growth processes of the films differ from those of MnBi-glass films prepared by the conventional vacuum evaporation. This can be attributed to the profound influence of ionized particles and the kinetic energy of the source materials.

The optical absorption coefficient α and the specific Faraday rotation F of the film were obtained to be 3.5×10^5 cm^{-1}

and 7.4×10^5 deg/cm, respectively at the wavelength of 6328 Å, resulting in the figure of merit $2F/\alpha = 4.5$ deg.

By using a He-Ne laser, Curie point writing could be successfully accomplished in the film. The diameter of written spot and the spot spacing were 2 μm and 5 μm, respectively realizing the recording density of 4×10^6 bit/cm^2. The written domains were found to be stable owing to the domain wall coercivity.

The Fourier power spectrum obtained from a line shape domain was observed and the calculated line width was in good agreement with the directly observed width under a polarizing microscope.

V MnNiBi FILMS

5.1 Introduction

Using the ICB technique, a ferromagnetic MnBi film with good uniformity over a large substrate area has been obtained, as described previous Chapter. From the practical use, however, MnBi films involve several problems, such as its relatively high Curie temperature ($\sim$360°C) and its phase transformation (from LTP to OHTP). Since a ferromagnetic compound $Mn_5Ni_2Bi_4$ has a moderate Curie temperature ($\sim$100°C)[95], a film of this material was prepared by the ICB technique.

In this chapter, crystallographic and magnetooptical properties of $Mn_5Ni_2Bi_4$ films obtained are described comparing with those of films prepared by the vacuum deposition.

5.2 Film Preparation

Preparation of $Mn_5Ni_2Bi_4$ films was made by using a multi crucibles type in the ICB technique. First, Ni was deposited on a glass substrate, and then Mn and Bi were simultaneously deposited. The composit films were overcoated with SiO protective layer, followed by annealing in air at temperatures up to 350°C. Typical conditions were acceleration voltage V_a= 3kV for the deposition of Ni, and V_a= 0.5kV for Mn and Bi, electron current for ionization I_e= 100mA and T_s (substrate temperature) = 140°C. The stoichiometry of the material was achieved by controlling the film thickness of 250 Å for Ni, and 1000Å for

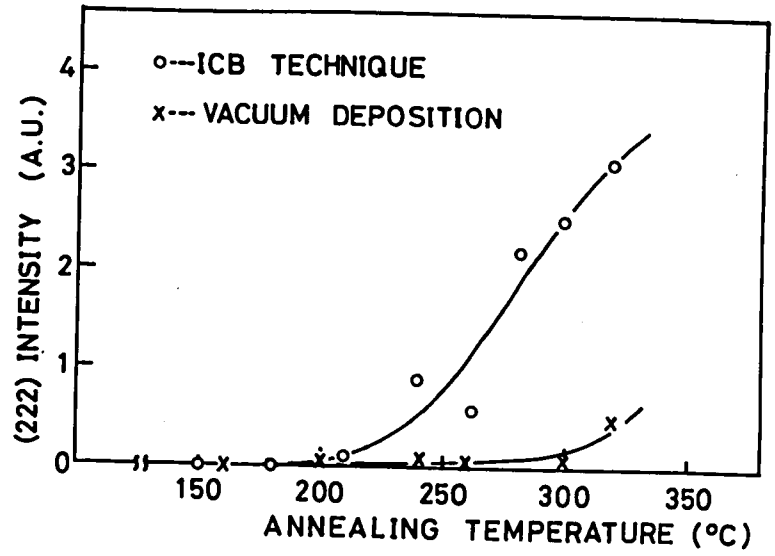

Fig. 5.1 Diffraction peaks of (222) plane as a function of annealing temperature.

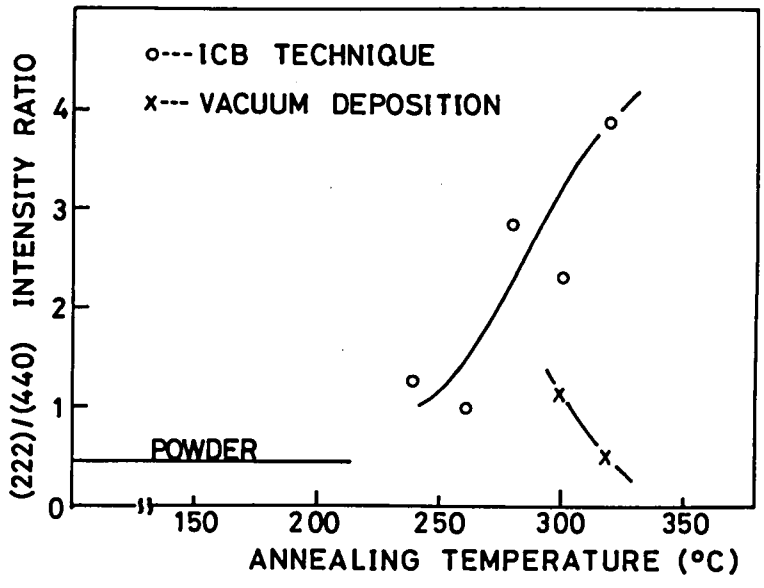

Fig. 5.2 Intensity ratios (222)/(440) as a function of annealing temperature.

Mn and Bi.

5.3 Evaluations of MnNiBi Films

5.3.1 Crystallographic Properties

Dependence of annealing temperatures on the crystal orientation was investingated by means of an X-ray diffraction. In Fig. 5.1, a change of the diffraction intensity of (222) plane in the film deposited by the ICB technique as a function of annealing temperature is compared with that of the film prepared by the vacuum deposition. In the case of the ICB-deposited film, the corresponding peak comes out at around 200°C. This temperature is apparently lower than that for the film by the vacuum deposition. The annealing films at elevated temperatures from 200°C to 350°C is found to increase the intensity of the peak. Figure 5.2 shows the intensity ratio (222)/(440) as a function of annealing temperature. In the ICB-deposited film, a preferential orientation of <111> axis perpendicular to the substrate surface increase with the annealing temperature, whereas in the vacuum-deposited film the ratio tends to decrease with increasing temperature, and finally becomes to the value of powdered sample. This result leads us to believe that the presence of ions and the kinetic energy of clusters produce the marked change in the critical condensation pressure of the source material, which is closely related to the nucleation and growth mechanism of the film. In fact, a MnNiBi film prepared by the vacuum deposition shows the X-ray diffraction pattern of two phases of MnBi and NiBi, which is reported by H.Gobel et al.[96)]

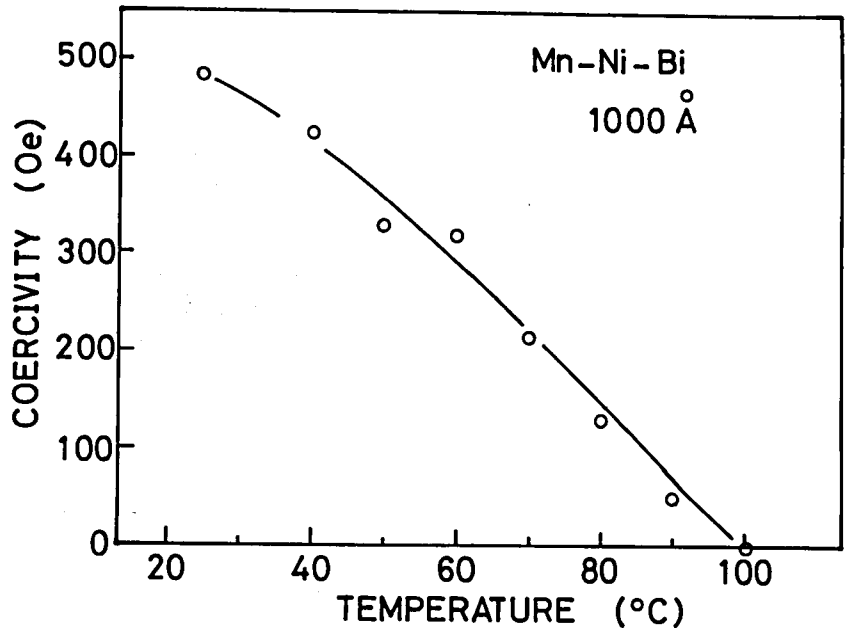

Fig. 5.3 The temperature dependence of the coercivity of $Mn_5Ni_2Bi_4$ film.

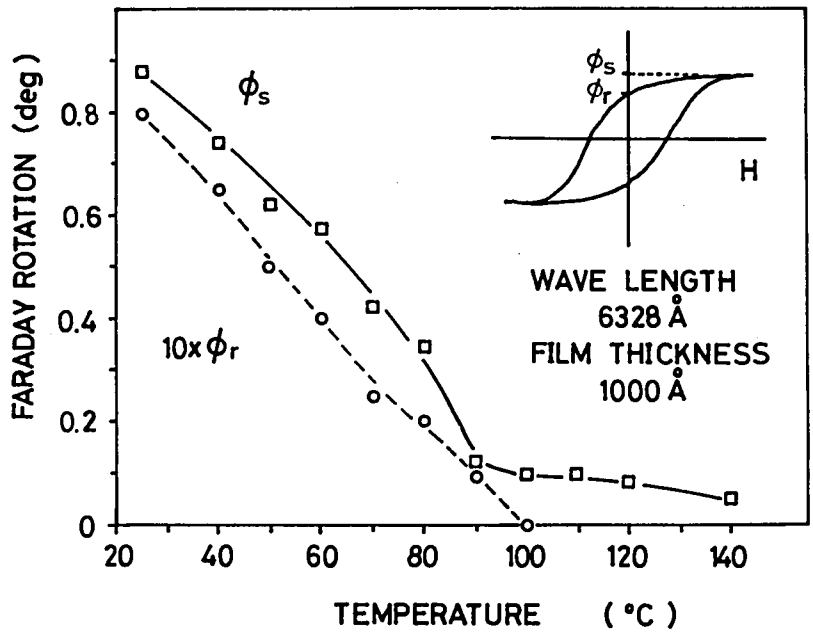

Fig. 5.4 The temperature dependence of the Faraday rotation of $Mn_5Ni_2Bi_4$ film.

In this study, there found no sign of such phase separation.

5.3.2 Magnetic and Optical Properties

The temperature dependence of the magnetic hysteresis curves of the annealed film were measured by means of Faraday effect to determine the Curie temperature. The results obtained are shown in Figs. 5.3 and 5.4. From the experiment, the Curie temperature of the $Mn_5Ni_2Bi_4$ film was determined to be about 100°C, which is in good agreement with the value of the powdered sample. The Faraday rotation at the saturated state ϕ_s, however, remains at the temperatures above 100°C suggesting the rotatory polarization due to a paramagnetic material and/or the short range ordering of magnetic spins in a paramagnetic state. The ratio ϕ_r/ϕ_s of magnetization at the remanent state ϕ_r and the saturated state ϕ_s is found to be 0.27 and the specific Faraday rotation is obtained with the wavelength of 6328Å to be 0.84×10^5 deg/cm at room temperature.

The optical properties are investigated as same as in the previous Chapter 4.3.2. The results of the transmissivity, the reflectivity at a substrate side R_g and at a SiO layer side R_s are shown in Fig. 5.5. By using Eq.(4.4), the optical absorption coefficient α is obtained, as shown in Fig. 5.6. From this result, the figure of merit of $Mn_5Ni_2Bi_4$ can be estimated.

The Curie temperature T_c, the specific Faraday rotation and the figure of merit at the wavelength of 6328Å of the $Mn_5Ni_2Bi_4$ film are compared with those of the MnBi film in

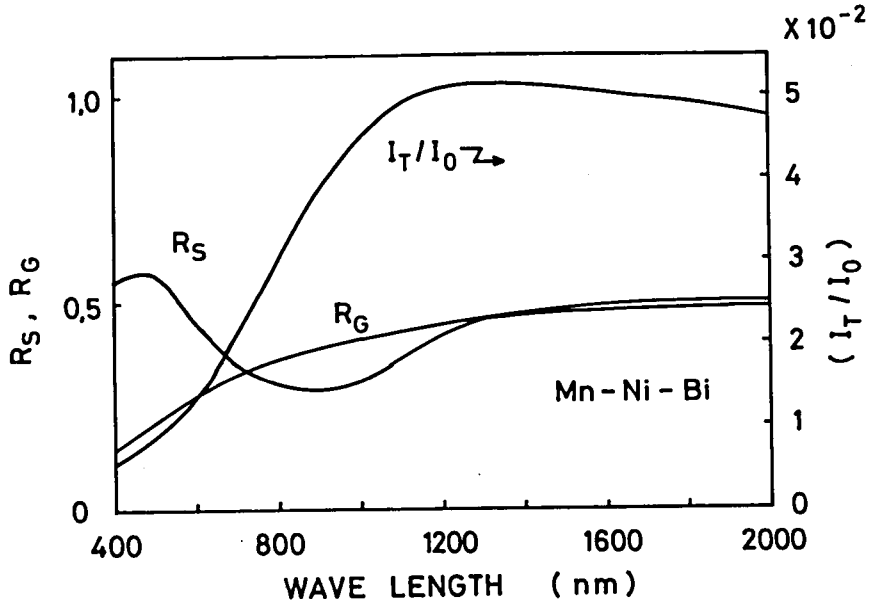

Fig. 5.5 The reflectivity and the transmissivity of $Mn_5Ni_2Bi_4$ film.

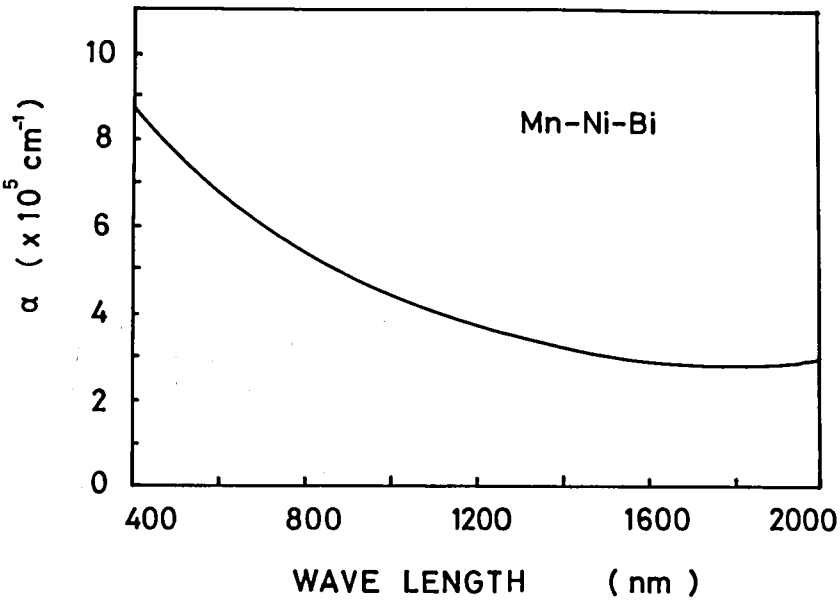

Fig. 5.6 The optical absorption coefficient α of $Mn_5Ni_2Bi_4$ film as a function of wavelength.

Table 5.1 Curie temperature T_c, the specific Faraday rotation F and the figure of merit $2F/\alpha$ of $Mn_5Ni_2Bi_4$ and MnBi films.

	T_c (°C)	F 10^5 (deg/cm)	$2F/\alpha$ (deg)
$Mn_5Ni_2Bi_4$	100	0.84	0.53
MnBi	360	7.4	4.5

Table 5.1. Apparently, these values of the $Mn_5Ni_2Bi_4$ film are smaller than those of the MnBi film. This can be explained by the fact that the values of exchange integral vary with the distance between two adjacent magnetic ions, as shown in Fig. 5.7[97], where "r_{ab}" is the distance between the nearest-neighbours, "r" is the ion radius, and "J_e" is exchange integral. For simplicity, we regard mainly Mn^{2+} ions as the magnetic ions associated with exchange integration. In the case of MnBi, the nearest-neighbour bonding between two Mn atoms aligns in the direction of c-axis, so that "r_{ab}" ≈ 3.0Å. Since the ion radius of Mn^{2+} is 0.8Å, the distance (r_{ab}- 2r) is 1.4Å. Consequently, the "J_e" becomes near the maximum, as shown in Fig. 5.7. On the contrary, in the case of $Mn_5Ni_2Bi_4$, the nearest-neighbour Mn^{2+} ions exist at the centers of octagonal and tetragonal sites, which are composed with Bi ions, as shown in Fig. 5.8. As seen in this figure, "r_{ab}" is 2.63Å, so that the distance (r_{ab}-2r) is 1.03Å. Consequently, the "J_e" becomes slightly positive suggesting that the bonding between two magnetic ions is very weak. The interpretation mentioned above is consistent with the experimental results, in which T_c and F of $Mn_5Ni_2Bi_4$ are lower than those of MnBi.

A measurement of ferromagnetic resonance (FMR) was made to determine the uniaxial anisotropic constant K_u at room temperature by employing the field modulation method and cylindrical cavity (H_{01} mode) at a frequency of 9.48 GH_z. Resonance equations are given by[98]

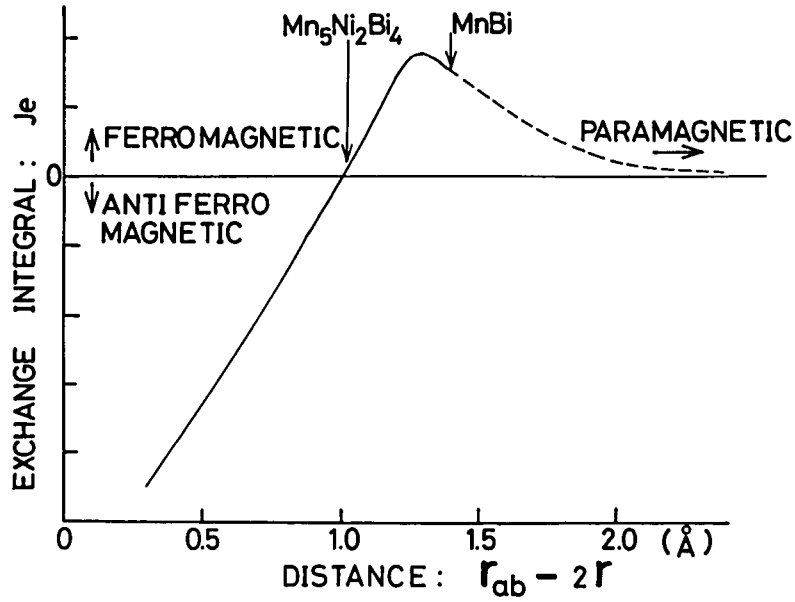

Fig. 5.7 Exchange integral as a function of the distance (r_{ab}- 2r).

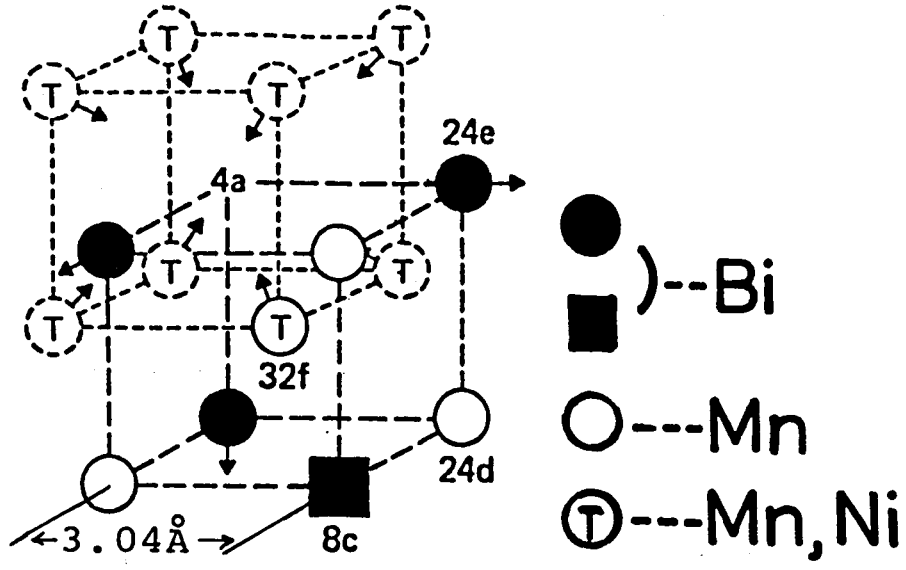

Fig. 5.8 Near- neighbour configuration of $Mn_5Ni_2Bi_4$.

$$H_{\perp} = \frac{\omega}{\gamma} - H_{eff} \qquad (5.1)$$

$$H_{//} = \frac{\omega}{\gamma} + \frac{1}{2} H_{eff} \qquad (5.2)$$

H_{eff}: the internal effective field

$$H_{eff} = 2K_u/M_s - 4\pi M_s \qquad (5.3)$$

where $H_{\perp}$ and $H_{//}$ are the resonance magnetic fields perpendicular and parallel to the film surface, respectively, ω is the angular frequency of microwave, γ the magneto-mechanical ratio and equals to $g\mu_B/\hbar$, M_s the saturation magnetization, K_u the uniaxial magnetic anisotropy constant. The values of g-factor and H_{eff} are determined by using Eqs.(5.1) and (5.2). It should be noted that a positive H_{eff} corresponds to the magnetization being perpendicular to the film surface.

Figure 5.9 shows the resonant magnetic field vs. the angle between the applied field and film surface. From the result, the internal effective field ($H_{eff} = 2K_u/M_s - 4\pi M_s$), was found to be -1667 (Oe). Taking into account of the value $4\pi M_s = 4.5 \times 10^3$ (Gauss/cm^3), K_u was determined to be 5.50×10^5 (erg/cm^3). That is, $K_u > 0$ and the magnetic easy axis aligns perpendicular to the substrate surface. The internal effective field, however, was actually negative because of the demagnetizing field, so that the magnetization did not align perpendicular to the substrate surface in the remanent magnetization. The experimental result that the observed Faraday rotation angle in the

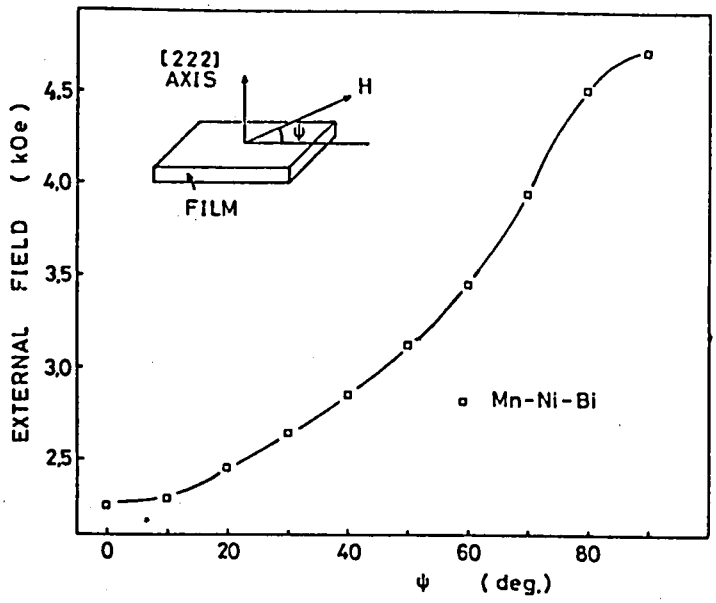

Fig. 5.9 Resonance magnetic field of $Mn_5Ni_2Bi_4$ film as a function of the angle ψ.

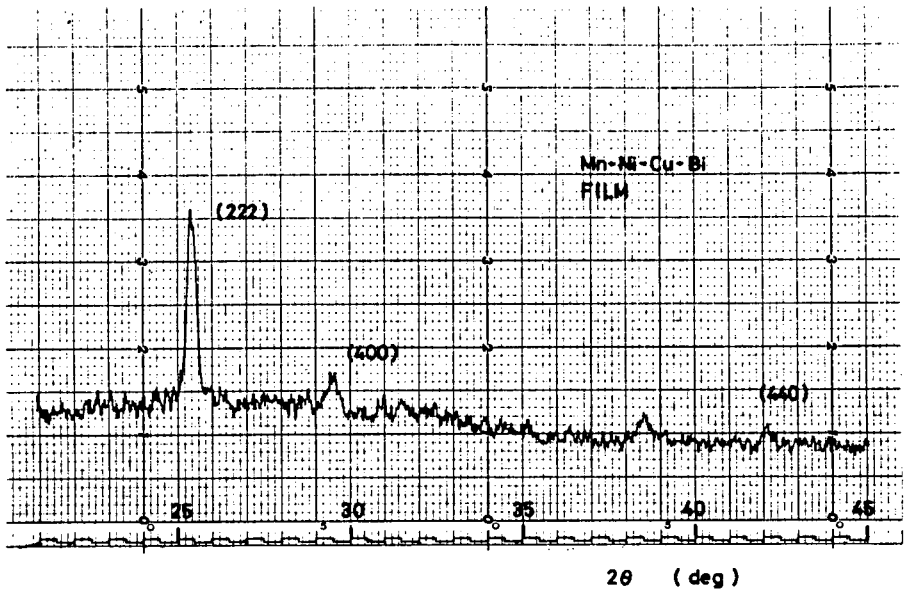

Fig. 5.10 X-ray diffraction pattern of Mn-Ni-Cu-Bi film.

remanent magnetization was 1/4 of that in the saturation magnetization is considered to indicate that the magnetization in this film did not align perpendicular to the substrate surface in the remanent magnetization.

5.4 Cu Doping

Since the magnetooptical recording system is convenient to be operated with no additional magnetic field in the reading process at room temperature, the remanent magnetization is desirable equal to the saturation magnetization for the maximum readout signal, which in other words the rectangular hysteresis is required as mentioned in Chapter II. Since copper is a paramagnetic material at room temperature, it is expected with the doping copper into the Mn-Ni-Bi film that the saturation magnetization decreases and as a result the internal effective field H_{eff} increases in accordance with Eq.(5.3) without the change of the crystal structure because the crystal structure is found to be face centered cubic in Mn-X-Bi system (X = Ni, Pd and Cu) [95),99)].

The Mn-Ni-Cu-Bi films were prepared as follows: First, Mn and Bi were deposited simultaneously on a glass substrate with the acceleration voltage V_a= 0.5 kV, and then Ni and Cu were deposited sequentially with the acceleration voltage V_a= 3 kV, followed by overcoating with a SiO layer. The thickness of Mn-Bi,Ni,Cu and SiO layer were about 400 Å, 100 Å, 100 Å and 2000 Å, respectively.

Figure 5.10 shows the X-ray diffraction pattern of the

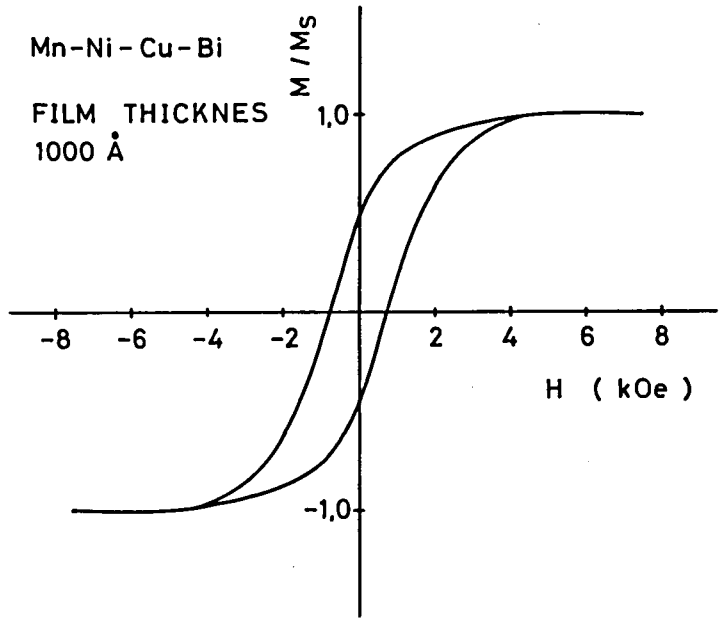

Fig. 5.11 The magnetic hysteresis of Mn-Ni-Cu-Bi film obtained by using the Faraday effect.

Mn-Ni-Cu-Bi film. The orientation to <111>-axis is most prominent. In Fig. 5.11, the magnetic hysteresis obtained by using the Faraday effect shows the ratio of magnetization at the remanent state and the saturated state as 0.48 which is greater than in the case of $Mn_5Ni_2Bi_4$ film by the factor of 1.8.

Figure 5.12 shows the result of the FMR measurement as compared with the case of the $Mn_5Ni_2Bi_4$ film. The resonance magnetic field is almost constant as 3.2 kOe. From Eqs.(5.1) and (5.2), we can obtain

$$H_{//} - H_{\perp} = \frac{3}{2}\left(\frac{2K_u}{M_s} - 4\pi M_s\right)$$

$$= \frac{3}{2} H_{eff} \qquad (5.4)$$

From the result of a constant resonance field,

$$H_{eff} = \frac{2K_u}{M_s} - 4\pi M_s \approx 0 \qquad (5.5)$$

is derived proving that the saturation magnetization M_s is decreased by Cu doping.

5.5 Summary

By using the ICB technique, $Mn_5Ni_2Bi_4$ films having a good orientation to <111>-axis could be successfully obtained. The Curie temperature of this material is found to be about 100 °C, and the specific Faraday rotation F, the figure of merit $2F/\alpha$ at the wavelength of 6328 Å are obtained to be 1.7×10^5 deg/cm

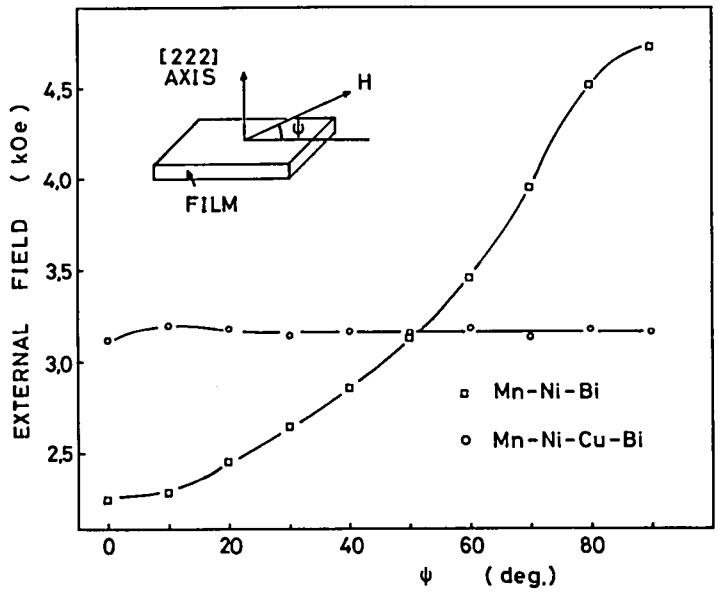

Fig. 5.12 Resonance magnetic field of Mn-Ni-Cu-Bi film as a function of the angle ψ.

and 0.53 deg., respectively. This lower values of the Curie temperature and the specific Faraday rotation are considered to be attributed to a small exchange integral.

With the doping of Cu into Mn-Ni-Bi film, the magnetization ratio of the remanent state and the saturated state is almost twice of the $Mn_5Ni_2Bi_4$ film and the internal effective field H_{eff} is increased from a negative to nearly zero because of the reduction of the saturation magnetization due to Cu doping.

VI GdFe FILMS

6.1 Introduction

Amorphous thin films of rare earth- transition metal (RE-TM) alloy have been investigated very intensively in recent years, because of interest in basic physics as well as practical application for bubble domain or thermomagnetic recording devices. A number of potential advantages exist for thermomagnetic applications of amorphous films. Large area memory plane can be readily prepared. The absence of crystalline structure reduces magnetostriction to the point where a very wide range of substrate are available. Optical properties, i.e., absorption and the Faraday rotation, seem to be adequate. Finally, the compensation temperature T_{comp} may be selected for optimum system performance. A number of questions about these new materials remain to be answered, e.g., stability and maximum areas of memory planes.

The first experimental observation of amorphous ferromagnetism was the work of A.Brenner et al. [100] in 1950 who observed ferromagnetic behavior in an amorphous film of Co-P prepared by electro-deposition. However, it was not until the mid 1960's that metallic amorphous materials received much attention [101]. Since then several amorphous materials have been prepared, primarily by one of four techniques: (1) Rapid quenching from the liquid state as for example in studies of Fe-Pd-P by P.L.Maitre-Pierre [102] and T.E.Sharon and C.C.Tuei [103], (2) Electrodeposition from solution as in the case of Ni-P [104]

and Co-P [105] alloys studied by G.S.Cargill and others, (3) Evaporation onto a cooled substrate as used by S.Fujima [106] and S.Mader and A.S.Norwick [107] to prepare amorphous alloys at low temperature which often recrystallize when heated to room temperatures, (4) D.C. triode sputtering system using a water cooled copper target as used for the neutron diffraction and magnetization studies of $TbFe_2$ [108].

Amorphous material are those showing no evidence of long-range atomic ordering. However, magnetic ordering has been observed in many of these materials [101]. Amorphous films produced over a wide composition range are single- phase metastable alloys. The magnetic ordering is an antiferromagnetic exchange coupling between the rare earth and transition metal sublattice, as is usually found in atomically ordered compounds of this type [109]. The uniaxial magnetic anisotropy field perpendicular to the film plane was reported to be well in excess of the demagnetizing field [110]. Various mechanisms have been proposed about the perpendicular anisotropy, such as the atomic pair orderings [111),112], micro-crystalline anisotropy [113),114], stress induced anisotropy [10),115] and anisotropyically shaped columnar arrays [116], but it has not been clarified the origin of the perpendicular anisotropy.

In this Chapter, the structural and magnetic properties of amorphous GdFe thin films prepared by the ICB technique have been studied by means of Auger analysis, X-ray diffraction and ferromagnetic resonance (FMR). As a result, some informations about the origin of the perpendicular anisotropy were obtained.

6.2 Film Preparation

Preparation of amorphous GdFefilms was made by the simultaneous deposition of Gd and Fe clusters onto a glass substrate, followed by overcoating with protective layer of SiO. Iron and gadolinium are heated at about 1600 °C and 1750 °C in each crucible with a small nozzle of 0.6 mm in diameter. The pressure maintained in the chamber is in the $1 \sim 5 \times 10^{-6}$ Torr range.

In this experiment, only iron clusters were ionized in order to investigate the influence of the iron ions especially on the pair coordination of atoms in the film. The electron current for ionization I_e and the acceleration voltage V_a were up to 300 mA and 0 V (with only ejection velocities of Fe clusters), respectively, and the substrate temperature T_s was about 200 °C. A total film thickness and a SiO layer were about 1500 Å and 1000 Å, respectively.

6.3 Evaluations of GdFe Films

The uniformity of deposited films were checked by means of Auger electron spectroscopy (AES). Figure 6.1(a) shows an example of the Auger spectrum of the film deposited with the condition $I_e \simeq$ 100 mA, $V_a \simeq$ 0 V, $T_s \simeq$ 200 °C. Figure 6.1(b) and (c) show the distribution of each component on the film surface and the depth profile. The GdFe films obtained were found to be entirely uniform over the large substrate area (about 5 x 5 cm^2) and also in the depth.

Figure 6.2 shows the SEM structure of a fractional edge of the GdFe film, sustaining the obious amorphous structure. It

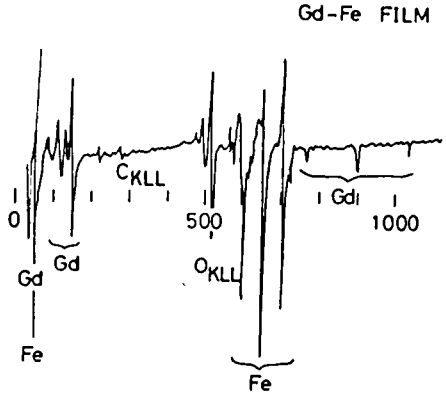

(a)

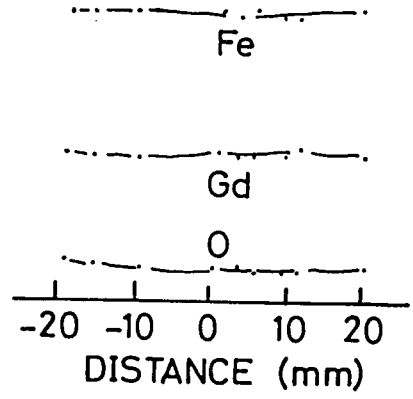

(b)

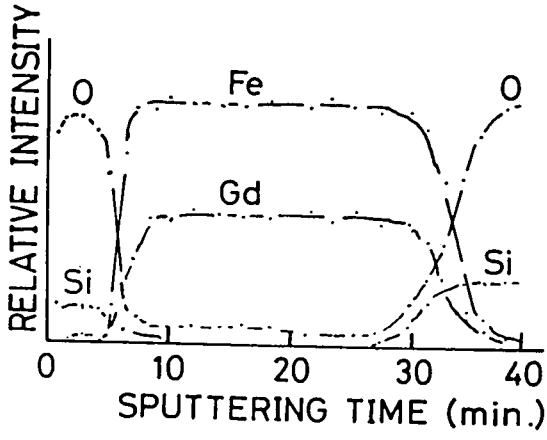

(c)

Fig. 6.1 (a) An example of the Auger spectrum of the GdFe film. (b) The distribution of each component of the GdFe film. (c) The depth profile of each component of the GdFe film.

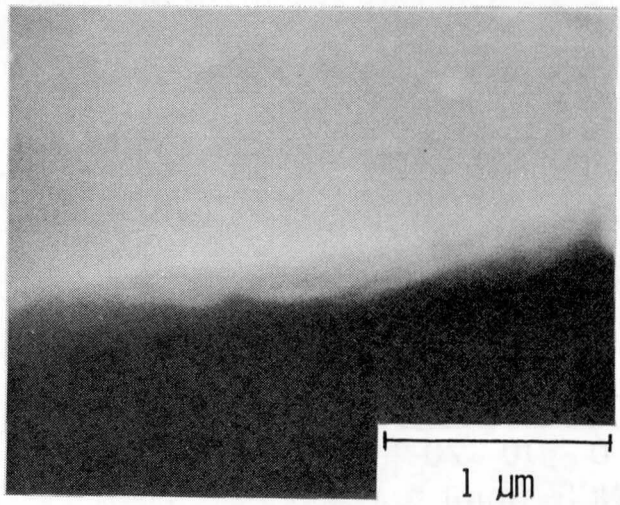

Fig. 6.2 SEM structure of a fractional edge of the GdFe film.

was also confirmed with the obtained film took a broad halo pattern being typical of the amorphous structure.

6.4 Structural Properties

Physical properties of amorphous film are closely related with the atomic pair coordination in the film. Measurements of X-ray diffraction were made for the purpose of obtaining the information about the atomic pair coordination, the interatomic distance and the coordination numbers.

The schematic diagram of the experimental equipment is shown in Fig. 6.3. A Rigaku diffractometer, Type RAD-IA generator, molybdenum or copper radiation, scintillation counter, bent graphite diffracted beam monochromator and pulse height analyzer were used for all intensity measurements. Firure 6.4 shows the typical diffraction patterns (Cu K_α) of GdFe films (Gd:Fe ≃ 1:3) at various electron currents for ionization I_e, where $s = 4\pi \cdot \sin\theta/\lambda$. These measures intensities, corrected for background, for polarization and for Compton modified scattering, were converted to electron units by the high angle method [117] to yield coherent intensity in electron units, $J_m(s)$. Following after Karle & Karle [118] together with a convergence method, $J_m(s)$ were converted to the interference function $J_z(s)$ using atomic scattering factors given in International Tables.[119] This interference function can be related to an reduced density function G(r) which is characteristic of the pair coordination in the isotropically diffracting materials. This relation is given by

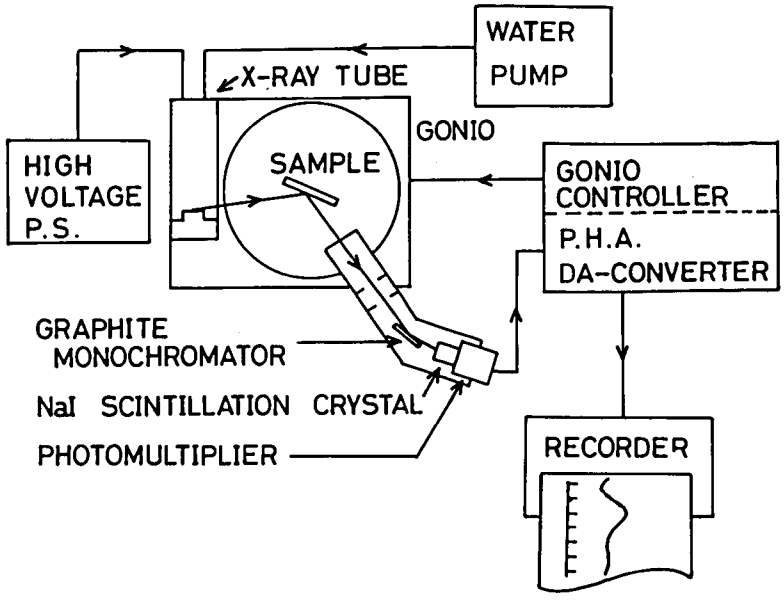

Fig. 6.3 The experimental equipment of X-ray diffraction measurement.

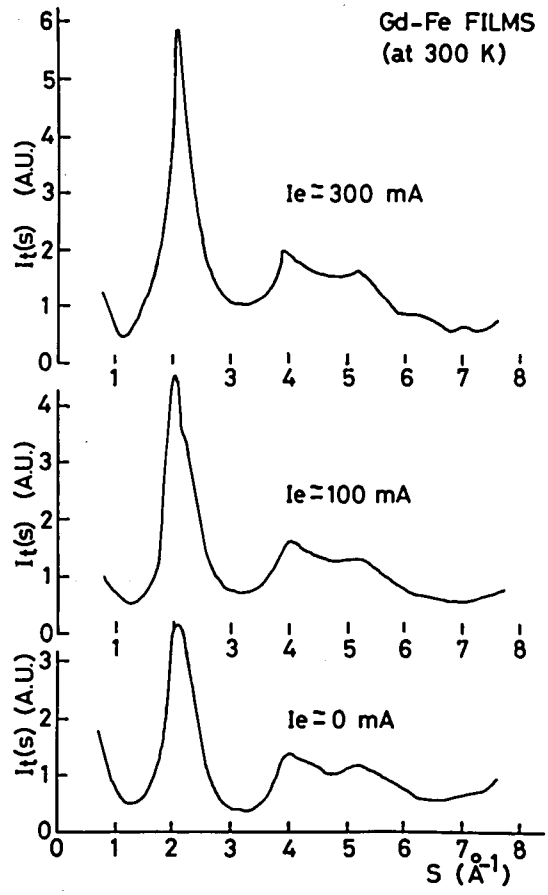

Fig. 6.4 The typical diffraction patterns of GdFe films at various electron current for ionization I_e.

$$G(r) = 4\pi r(\rho(r) - \rho_0)$$

$$= \frac{2}{\pi} \int_0^\infty s \cdot \exp(-\alpha s^2) \cdot J_z(s) \cdot \sin sr \, ds \qquad (6.1)$$

where ρ_0 is the average atomic density, and $\exp(-\alpha s^2)$ is the artificial temperature factor. The constant α can be determined by the following condition.

$$\exp(-\alpha s_{max}^2) \leq 0.1 \qquad (6.2)$$

where s_{max} is the maximum value of s. In this experiment, s_{max} is 17.36 $\mathring{A}^{-1}$ because λ is 0.7107 $\mathring{A}$ for Mo K_α and the maximum 2θ is limited at 158° by the equipment used, which correspond to $\alpha = 0.008$.

Figure 6.5 shows the results of G(r) obtained with the films shown in Fig. 6.4. Taking account of the radii of Gd, Fe atoms (Gd = 1.78 $\mathring{A}$, Fe = 1.27 $\mathring{A}$), the nearest-neighbour bonding peaks corresponding to Fe-Fe, Gd-Fe, and Gd-Gd pairs lie in that order, and the value of r is nearly the sum of radii of two atoms. The peak around r ≈ 5 $\mathring{A}$ corresponds to the multiple coupling of Fe atoms. Comparing the result of I_e ≈300 mA with the case of I_e ≈ 0 mA in Fig. 6.5, the Fe-Fe pair density is reduced by the presence of Fe ions. Furthermore, the Gd-Fe pair density is dominant even for the film deposited with neutral clusters alone, suggesting that the kinetic energy of clusters and the migration effect on a substrate surface enhance the

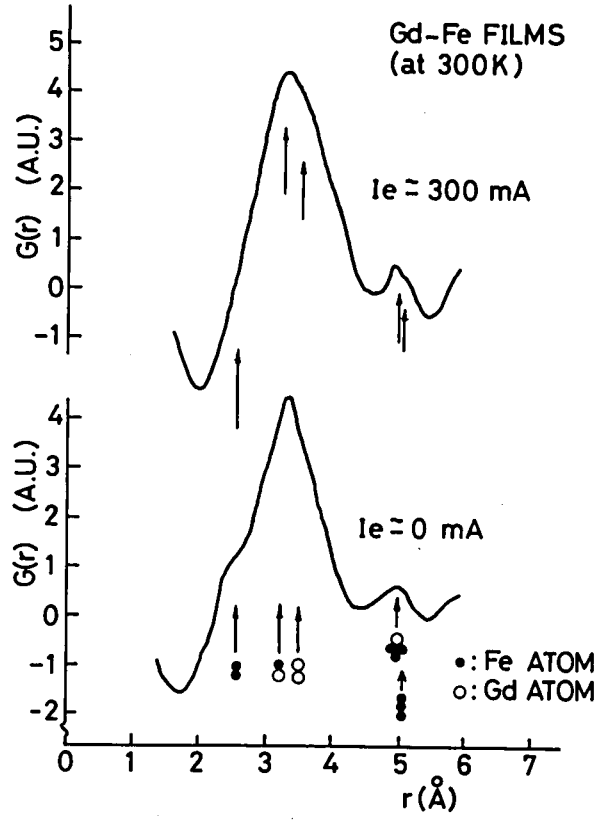

Fig. 6.5 Reduced density functions G(r) of GdFe films (Gd:Fe ≈ 1:3).

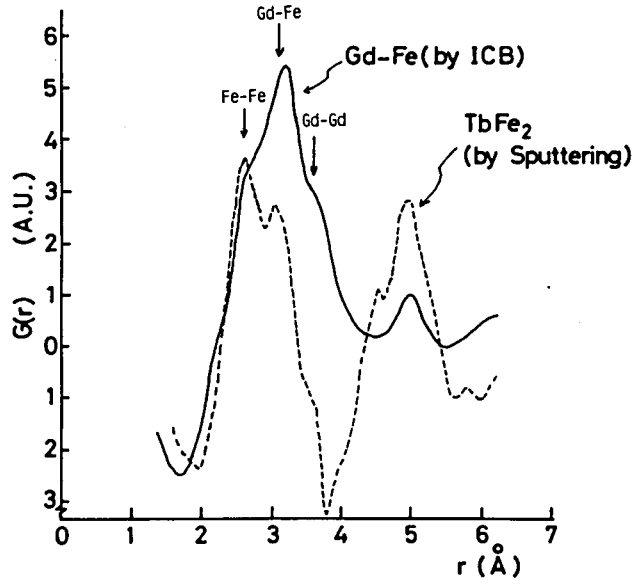

Fig. 6.6 Reduced density functions G(r) of GdFe film prepared by the ICB technique as compared with the $TbFe_2$ film by sputtering method.

coupling of different species. In fact, the $TbFe_2$ amorphous film prepared by sputtering method where the impinging particles are neutral and their kinetic energy is smaller than those of the ICB technique, the Fe-Fe pair density is rather large as shown in Fig. 6.6.

Figure 6.7 shows the results of G(r) obtained with the films ($I_e \simeq 300$ mA) at various atomic ratio of Gd and Fe. The peak around $r \simeq 5$ Å reduces with the atomic ratio reaching to nearly 1:1,while the Gd-Fe pair is dominant and does not change.

6.5 Magnetic Properties

In order to investigate the magnetic properties of GdFe films, especially on the magnetic anisotropy of the films, measurements of a ferromagnetic resonance (FMR) were made at room temperature, as in the Chapter 5.3.2.

Figure 6.8 shows the FMR spectra of GdFe films (Gd:Fe ≃ 1:3) at various electron currents for ionization I_e. Since the Fe-Fe pair density was reduced by the presence of ion and the Gd-Fe pair is dominant as shown in Fig. 6.5, the spin-wave resonance takes place in the case of Fig. 6.8(c) ($I_e = 300$ mA). The resonance equation of the spin-wave pinned at both the substrate and film surface sides is given by

$$\omega_k = \gamma\{H + H_m a^2 \left(\frac{\pi}{d}\right)^2 n^2\} \qquad (6.3)$$

where ω_k is the resonance angular frequency, γ is the magneto-mechanical ratio, H the external magnetic field, H_m the molecu-

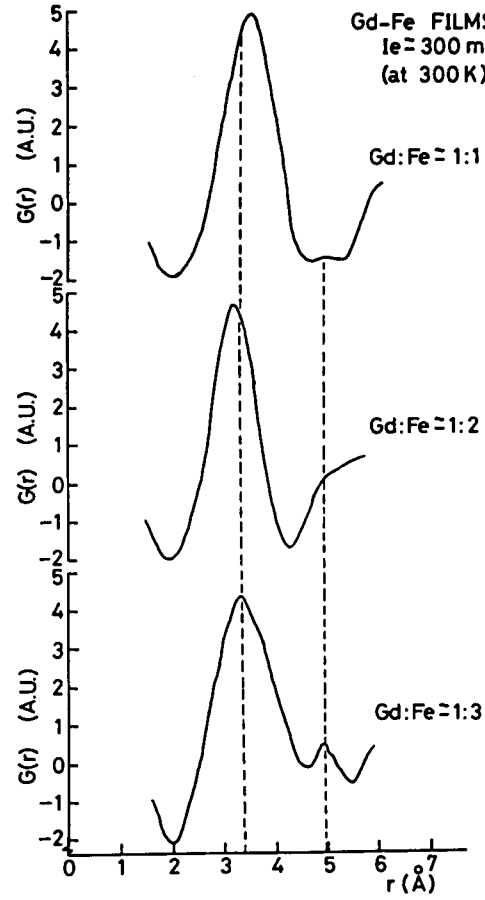

Fig. 6.7 Reduced density functions G(r) of GdFe films ($I_e \simeq$ 300 mA).

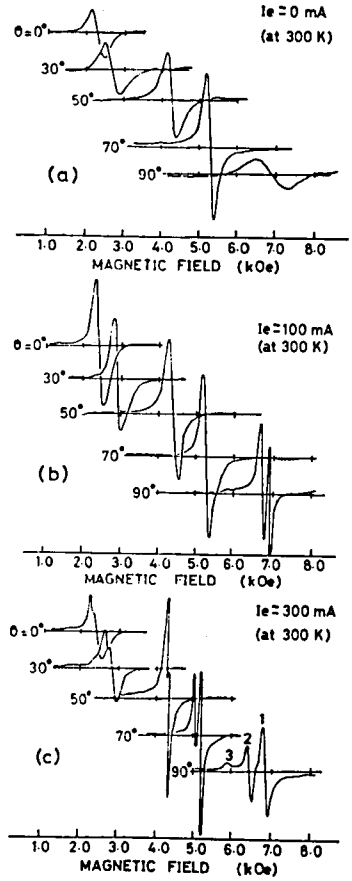

Fig. 6.8 FMR spectra of GdFe films (Gd:Fe ≃ 1:3).

lar field, a is the distance of spins, d the film thickness, and n is the resonance mode. In Fig. 6.8(c), the FMR spectrum of $\theta = 90°$ exhibits three resonance peaks denoted as 1, 2 and 3. Judging from the resonance field, the peaks of 1, 2 and 3 correspond to 0th, 3rd and 4th mode of the spin-wave resonance, respectively. Applying $a \simeq 3.2$ Å (the interatomic distance of Gd-Fe) and $d = 2700$ Å into Eq.(6.3), the values of H_m can be estimated to be $H_m \simeq 2.86 \times 10^6$ Oe. By using the relation between the molecular field and the exchange stiffness constant A, which is

$$H_m \cdot a = 2A/M_s \tag{6.4}$$

the exchange stiffness constant A was determined to be $A \simeq 0.35 \times 10^{-6}$ erg/cm where M_s is taken as 200 Gauss. This value is in good agreement with the results of $GdFe_2$ films obtained by T.Katayama et al. [8] where the exchange stiffness constant was determined by following formula.

$$\sigma_w = 4\sqrt{A \cdot K_u} \tag{6.5}$$

where σ_w is the energy density of domain wall.

Figure 6.9 shows the FMR spectra of GdFe films ($I_e = 300$ mA) at various atomic ratio. The internal effective field H_{eff}, g-factor and uniaxial magnetic anisotropy constant were obtained by using Eqs.(5.1) and (5.2), M_s being taken as 200 Gauss. The results are given in Table 6.1. The internal effective

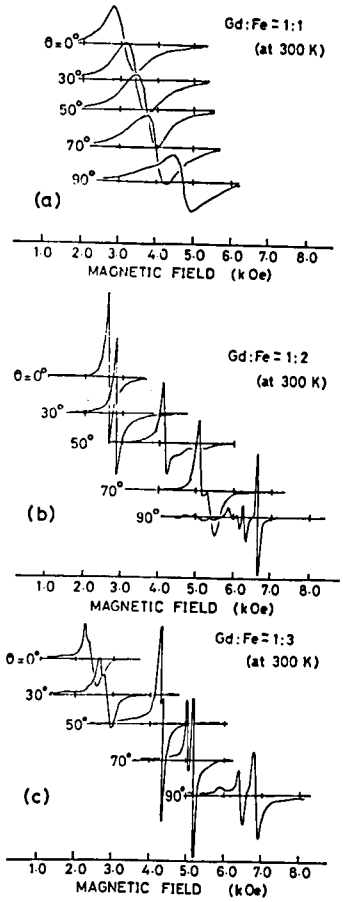

Fig. 6.9 FMR spectra of GdFe films ($I_e \simeq 300$ mA).

Table 6.1 The values of H_{eff}, K_u, g of Gd-Fe films at various Gd/Fe ratio

Gd : Fe	1 : 1	1 : 2	1 : 3
H_{eff} (kOe)	-1.10	-2.61	-3.91
K_u (erg/cm^3)	1.42×10^5	-8.67×10^3	-1.40×10^5
g	1.83	1.70	1.67

field H_{eff} increases with the atomic ratio reaching to 1:1 and the uniaxial magnetic anisotropy constant K_u is positive when the atomic ratio Gd:Fe = 1:1. This aspect is similar to the case of $Mn_5Ni_2Bi_4$ films as described in Chapter 5.3.2. This increases of H_{eff} and K_u correspond to the reduction of multiple coupling of Fe atoms as shown in Fig. 6.7. The dependency of K_u on film composition was also observed in the film prepared by R.F. sputtering method [120),121)]. From the results mentioned above, the multiple coupling of Fe atoms is likely the cause of the reduction of uniaxial magnetic anisotropy constant K_u.

6.6 Bi Doping

By using the ICB technique, GdFe films showed that the Gd-Fe pair was dominant in a film even when 30% of Fe clusters were included and that the internal effective field H_{eff} were negative, as described previous section.

In this section, Bi doped GdFe films prepared by using the ICB technique are evaluated from the standpoint of uniformity, and the results of measurements on X-ray diffraction and FMR of the films are described, and the effect of Bi doping are discussed.

Preparation of Bi doped GdFe films was made by the deposition of Gd and Fe clusters and the simultaneous evaporation of Bi onto a glass substrate, followed by overcoating with a SiO layer. The iron and gadolinium vapours are ejected into a vacuum chamber together with bismuth vapour from an other

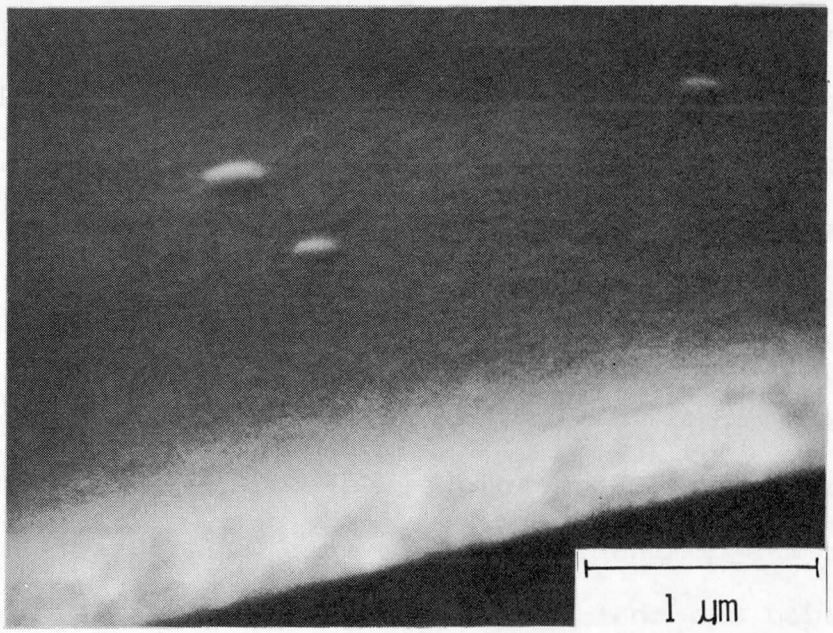

Fig. 6.10 SEM structure of a fractional edge of the Bi doped GdFe film.

conical tungsten filament located between two cluster sources, and the pressure maintained in the chamber is in the 3 ∿ 6 x 10^{-6} Torr range.

In this experiment, only iron clusters were ionized as same as the previous section. The electron current for ionization I_e and the acceleration voltage V_a were 300 mA and 0 V (with only ejection velocities of Fe clusters), respectively, and the substrate temperature T_s was about 200 °c. A total film thickness and a SiO layer were 2000 ∿ 3000 Å and 1000 ∿ 1500 Å, respectively. The Bi doped GdFe films investigated were analyzed by X-ray microprove analysis. With keeping the concentration of Gd and Fe at 50 atomic per cent (at.%), the content of Bi was varied up to 22.2 at.% with the composition of $(GdFe)_{1-x}Bi_x$. The uniformity of deposited film were checked by AES and were found to have the good uniformity as in the case of GdFe films.

Figure 6.10 shows the fractional edge of a Bi doped GdFe film, sustaining the obvious amorphous structure. Also it was confirmed with the result of X-ray diffraction study that the obtained film took broad halo patterns being typical of the amorphous structure.

Figure 6.11 shows the results of G(r) obtained with the pure GdFe film and the Bi doped (Bi 22.2 at.%) GdFe film. Taking account of the radii of Gd,Fe, Bi atoms (1.78 Å, 1.27 Å and 1.55 Å), the non-discrete broad peak in G(r) of the Bi doped GdFe film around 3 Å around which the nearest-neighbour bonding peak exists are mixed together with Gd-Fe,Fe-Fe,Gd-Gd,Gd-Bi,

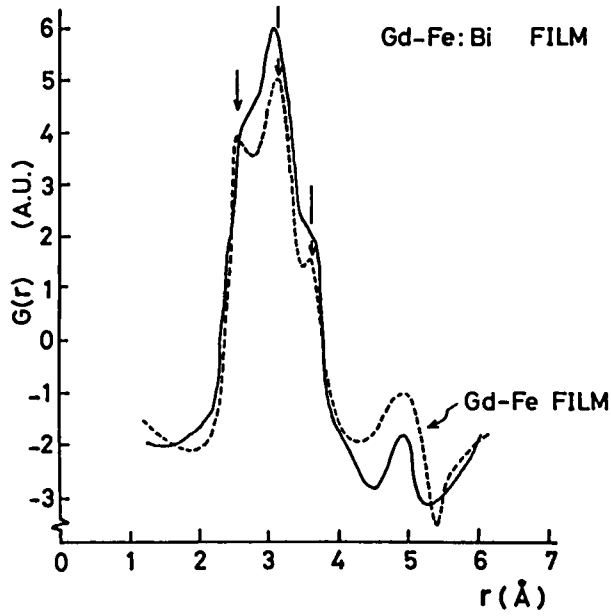

Fig. 6.11 Reduced density functions G(r) of GdFe and Bi doped GdFe films.

and Bi-Bi pairs because the three peaks corresponding to Fe-Fe, Gd-Fe and Gd-Gd pairs obtained with the pure GdFe film are separated clearly. It should be noted that Gd-Fe pair is dominant for films prepared by the ICB technique.

Bi doped GdFe films were then annealed in vacuum for one hour at 260 °C. As a result , the value of the internal effective field H_{eff} of the film were found to become positive, proving the positive perpendicular anisotropy. Figures 6.12 and 6.13 show the results of G(r) obtained with the films of Bi 5.4 at.% and 22.2 at.%, respectively. In both cases, the shoulders of non-discrete broad peak are found to shift toward longer values of r by annealing and it is marked for the films of high Bi concentration. From the results, it is suggested that Gd-Bi pair increase and Fe-Bi pair decrease by the annealing.

In order to investigate the magnetic properties of Bi doped GdFe films, FMR measurements were made as in the same way of the previous section. Figure 6.14 shows the internal effective field H_{eff} and the peak to peak value of absorption intensities I_{pp} of GdFe films with different concentration of Bi, where open circle are the values of as-deposited films and closed circles are those of annealed films. The value of H_{eff} of the as-deposited film increase with the doping of Bi and gradually increase to a positive value as the Bi content increases. On the other hand, I_{pp} was considerably decreased by doping of Bi about 5.0 at.%. The result suggests that the doping of Bi into GdFe film plays a significant role in decreasing the saturation

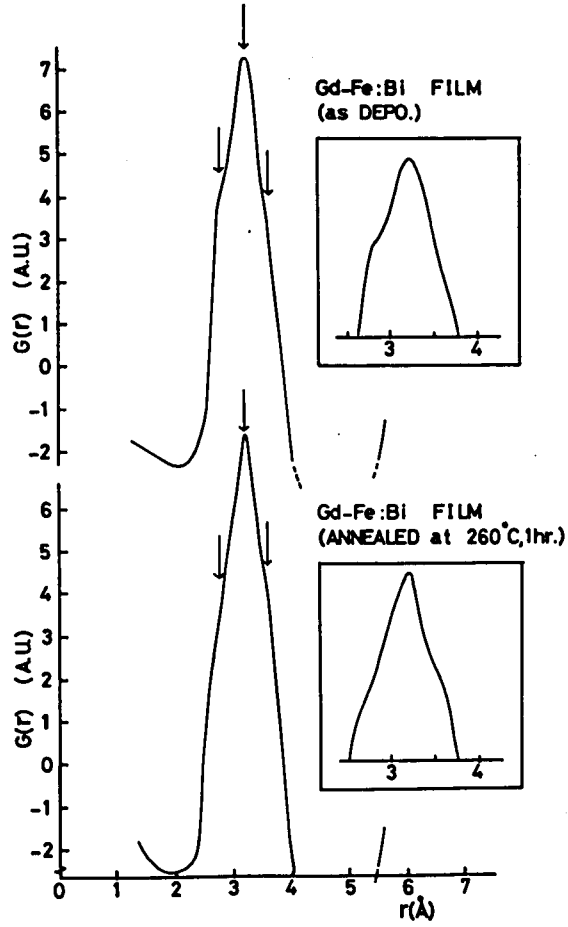

Fig. 6.12 Reduced density functions G(r) of the GdFe:Bi film of Bi 5.4 at.%.

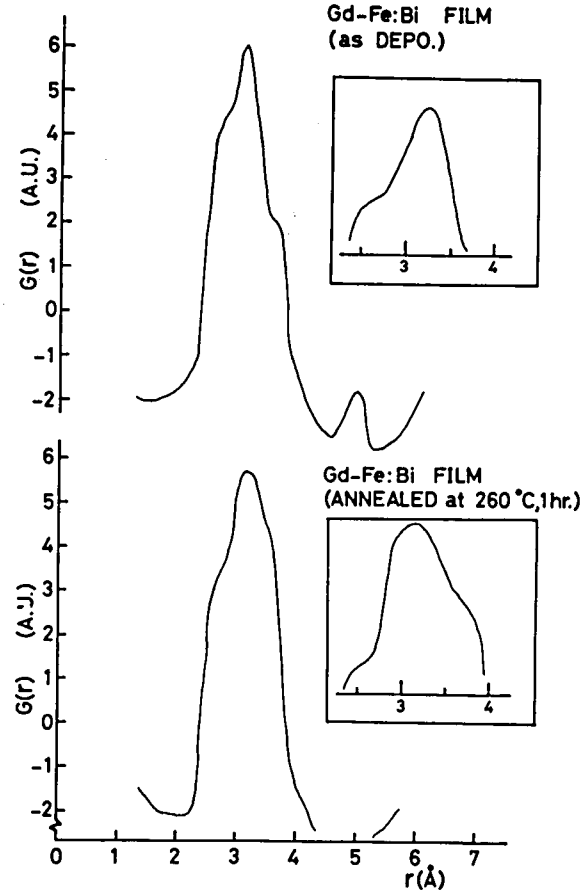

Fig. 6.13 Reduced density functions G(r) of the GdFe:Bi film of Bi 22.2 at.%.

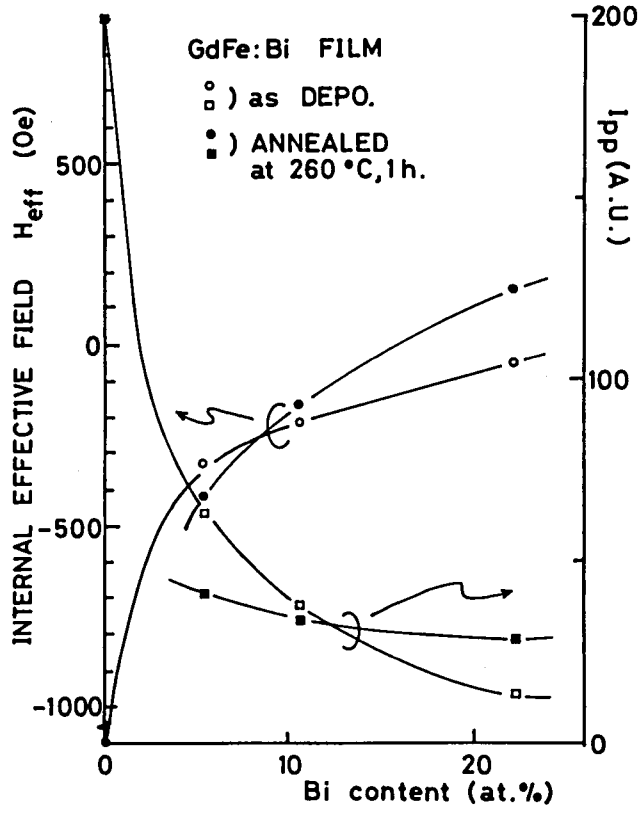

Fig. 6.14 The internal effective field H_{eff} and the peak to peak value of the absorption intensities I_{pp} of GdFe films with different consentration.

tion magnetization M_s, resulting in a marked increase of H_{eff}. As regards I_{pp}, it is considered that the exchange interaction between magnetic spins is weakened by the Bi doping. The values of H_{eff} of the annealed film of Bi 22.2 at.%, as compared with the as-deposited films, is greater and turns into positive sign, that is, the magnetization being perpendicular to the film surface. Taking account of the results of X-ray diffraction study, the value of G(r) at a larger value of r than 3.2 Å (Gd-Fe interatomic distance) is found to be related to the increase of H_{eff} after annealing.

The g-factor of the Bi doped GdFe films are tabulated in Table 6.2. These values are discussed in terms of the Tsuya-Wangsness formura [122)-124)] which should be applied to all of the ferrimagnetic material. The Tsuya-Wangsness formula of the $Gd_{1-x}Fe_x$ is expressed as

$$g = \frac{(1-x)M_{Gd} - xM_{Fe}}{(1-x)\frac{M_{Gd}}{g_{Gd}} - x\frac{M_{Fe}}{g_{Fe}}} = \frac{(1-x) - xR}{(1-x)\frac{1}{g_{Gd}} - x\frac{R}{g_{Fe}}} \qquad (6.6)$$

where $R = M_{Fe}/M_{Gd}$, g_{Gd} and M_{Gd} are g-factor and magnetization of Gd sublattice, and g_{Fe} and M_{Fe} are those of Fe sublattice, respectively.

The compensation temperature T_{comp} for impurity free GdFe films decreased as the content of Fe increased [12)], while the T_{comp} for Bi doped GdFe films decreased with increasing the concentration of Bi [125)]. From these facts, the doping of Bi into GdFe films can be regarded equivalently as an increase of

Table 6.2 g-factors of Bidoped GdFe films at various Bi content

Bi at.%	5.4	10.6	22.2
as-depo.	2.01	2.01	2.01
annealed	1.95	2.00	2.08

x in Eq.(6.6). In this study, x was kept constant at 0.5 so that we can examine the value of R since an increase of x is equivalent to an increase of M_{Fe} and a decrease of M_{Gd}, which lead to as increase of R. The annealing of Bi doped GdFe films leads to increase M_{Fe} and to decrease M_{Gd}, which correspond to the results of X-ray diffraction study in which Fe-Bi pair decreased and Gd-Bi pair increased by annealing.

Applying x = 0.5, g_{Gd} = 2.02 [126], g_{Fe} = 2.065 [126] and the g-factors obtained in Table 6.2 into Eq.(6.6), the values of R could be estimated to be R = 0.186 for the as-deposited films, 4.09 for the annealed film of Bi 22.2 at.%, and 0.622 for the annealed film of Bi 5.4 at.%. This is reasonable by comparing the result that the shift of the shoulders in G(r) obtained from X-ray diffraction was more intense for the film of Bi 22.2 at.% than for that of Bi 5.4 at.%. Supposing $g_{Fe} > g_{Gd}$, the g-factor of Bi doped GdFe films decrease with increasing the value of R as seen in Eq.(6.6). This will be applied to the annealed film of Bi 5.4 at.%, but can not be applied to the annealed film of Bi 22.2 at.%. In the latter case, the g-factor was rather great than that of the as-deposited film. The shift of shoulders, that is from Fe-Bi pairs to Gd-Bi pairs, of the film of Bi 5.4 at.% was nearly done by annealing, while the shoulder corresponding Fe-Bi pairs of the film of Bi 22.2 at.% still remained even after annealing, as seen in Figs. 6.12 and 6.13. This can be attributed to the large g-factor of the annealed film of Bi 22.2 at.%, or an influence of Bi on the molecular field between Gd and Fe atoms.

6.7 Summary

Film formation of GdFe with a uniform amorphous structure were performed using the ICB technique. The films obtained were completely uniform over the area of 5 x 5 cm^2 and through their thickness. The presence of ions and the kinetic energy of vapourized metal clusters are likely cause of the uniform amorphous structure of films even when the iron clusters were alone ionized.

From the measurements on the X-ray diffraction, it was found that the Gd-Fe pair is dominant for the films prepared by the ICB technique. As a result, the spin-wave resonance was observed in the FMR spectra. This was confirmed by calculating the molecular field and the exchange stiffness constant using the resonance equation of spin-wave.

The multiple coupling of Fe atoms in a film was considered to be a cause of the reduction of uniaxial magnetic anisotropy.

For the Bi doped GdFe films, it was found that the shift of shoulders in G(r) corresponding with the change from Fe-Bi pairs to Gd-Bi pairs is observed by annealing more clearly as Bi content was increased. From the measurements on FMR, it was found that the internal effective field H_{eff} was markedly increased by Bi doping and became positive by annealing. The annealing effect by which H_{eff} became positive is closely related to the shift of shoulders in G(r). Applying the Tsuya-Wangsness formula, the sublattice moment ratio $R = M_{Fe}/M_{Gd}$ were estimated to be o.186, 4.09 and 0.622 for the as-deposited films of various Bi content, the annealed film of Bi 22.2 at.%,

and the annealed film of Bi 5.4 at.%, respectively.

Detailed analysis of the pair coordination of components and the sublattice moments, g-factor should be done under the ion content, ion species, and the energy of the ionized cluster beam.

VII CONCLUDING REMARKS

Magnetic thin films prepared by ionized cluster beam technique have been studied with respect to their crystallographic and magnetic properties. By using ICB technique, the physical and crystallographic characteristics of the deposited films can be adjusted suitably for the magnetooptical recording material by controlling deposition parameters according to the source and substrate material.

In Chapter II, a general idea of magnetooptical recording and requirements on material used in such recording process have been reviewed. Optical writing and reading processes have summarized and ultimate recording density for MnBi is obtained to be 10^{10} bits/cm^2.

In Chapter III, mechanisms of cluster formation have described and the characteristics of the practical ICB source used in preparing films have been mentioned in a case of Mn and Bi sources.

From Chapter IV through VI, individual magnetic films have been investigated in detail. For MnBi films, large scale uniaxial thin films suitable for thermomagnetic recording application could be successfully obtained. The films were easily prepared by a simultaneous method of the ICB deposition of Mn and Bi onto a glass substrate, and found to be extremely uniform over a large area and easily reproducible. The nucreation and crystal growth processes of the films differ from those of MnBi-glass films prepared by the conventional vacuum evaporation. This can be attributed to the profound influence of ionized particles and the kinetic energy of the source materials.

The optical absorption coefficient and the specific Faraday rotation F of the film were obtained to be 3.5×10^5 cm^{-1} and 7.4×10^5 deg/cm, respectively at the wavelength of 6328 Å, resulting in the figure of merit $2F/\alpha$ = 4.5 deg.

By using a He-Ne laser, Curie point writing could be sucessfully accomplished in the film. The diameter of written spot and the spot spacing were 2 μm and 5 μm, respectively, realizing the recording density of 4×10^6 bit/cm^2. The written domains were found to be stable owing to the domain wall coercivity.

The Fourier power spectrum obtained from a line shape domain was observed and the calculated line width was in good agreement with the directly observed width under a polarizing microscope.

For MnNiBi films, a good orientation to <111>-axis could be obtained. The Curie temperature of this material is found to be about 100 °C, and the specific Faraday rotation F, the figure of merit $2F/\alpha$ at the wavelength of 6328 Å are obtained to be 1.7×10^5 deg/cm and 0.53 deg, respectively. This lower values of the Curie temperature and the specific Faraday rotation are considered to be attributed to a small exchange integral.

With doping of Cu into Mn-Ni-Bi film, the magnetization ratio of the remanent state and the saturated state is almost twice of the $Mn_5Ni_2Bi_4$ film and the internal effective field H_{eff} is increased from a negative to nearly zero because of the reduction of the saturation magnetization due to Cu doping.

For GdFe films, a uniform amorphous structure have performed over a large area and their entire thickness. From the measurements on the X-ray diffraction, it was found that the Gd-Fe pair

is dominant for the films prepared by the ICB technique. As a result, the spin-wave resonance was obtained in the FMR spectra. This was confirmed by calculating the molecular field and the exchange stiffness constant using the resonance equation of spin-wave.

The multiple coupling of Fe atoms in a film was considered to be a cause of the reduction of uniaxial magnetic anisotropy.

For the Bi doped GdFe films, it was found that the shift of shoulders in G(r) corresponding with the change from Fe-Bi pairs to Gd-Bi pairs is observed by annealing more clearly as Bi content was increased. From the measurements on FMR, it was found that the internal effective field H_{eff} was markedly increased by Bi doping and became positive by annealing. The annealing effect by which H_{eff} became positive is closely related to the shift of shoulders in G(r). Applying the Tsuya-Wangsness formula, the sublattice moment ratio $R = M_{Fe}/M_{Gd}$ were estimated to be 0.186, 4.09 and 0.622 for the as-deposited films of various Bi content, the annealed film of Bi 22.2 at.%, and the annealed film of Bi 5.4 at.%, respectively.

From the results obtained in this thesis, the Ionized Cluster Beam (ICB) technique was found to have a great ability to be used in preparing magnetic thin films for magnetooptical recording. The role of ions in film formation is predominant and the film characteristic can be controlled easily.

The ICB technique has many features which are promissing for magnetic thin film formation, especially for intermetalic compounds. From the standpoint that in intermetalic magnetic

material, magnetic spins are coupled each other rather directly than oxide magnetic material in which spins are coupled through a anion, many applications for these material have been considered by using the ICB technique taking into account in its direct controllability on film formation.

References

1) D.Chen, J.F.Ready and E.Bernal G., J. Appl. Phys., 39(1968) p.3916.

2) R.L.Aagard, F.M.Schmit, W.Walters and D.Chen, IEEE Trans. on Magn., MAG-7(1971) p.380.

3) G.W.Lewicki, IEEE Trans. on Magn., MAG-5(1969) p.298.

4) W.K.Unger and R.Räth, IEEE Trans. on Magn., MAG-7(1971) p.885.

5) B.Tsujiyama, S.Yoshii and K.Nishiguchi, IEEE Trans. on Magn., MAG-8(1972) p.603.

6) W.K.Unger and M.Stolz, J. Appl. Phys., 42(1971) p.1085.

7) H.Schröder et al., Phys. Stat. Sol., (a)5(1971) p.169.

8) T.Katayama, K.Hasegawa, K.Kawanishi and T.Tsushima, J. Appl. Phys., 49(1978) p.1759.

9) C.Vittoria, P.Lubitz and V.Ritz, J. Appl. Phys., 49(1978) p.4908.

10) T.Katayama, M.Hirano, Y.Koizumi and T.Tsushima, IEEE Trans. on Magn., MAG-13(1977) p.1603.

11) N.Imamura, Y.Mimura and T.Kobayashi, J. Appl. Phys., 48 (1977) p.2634.

12) A.Gangulee and R.C.Taylor, J. Appl. Phys., 49(1978) p.1762.

13) M.Amatsu, S.Honda and T.Kusuda, IEEE Trans. on Magn., MAG-13 (1977) p.1612.

14) S.Matsushita, K.Sunago and Y.Sakurai, IEEE Trans. on Magn., MAG-11(1975) p.1109.

15) T.Takagi, K.Matsubara, H.Takaoka and I.Yamada, Thin Solid Films, 63(1979) p.41.

16) Chr.Weissmantel, Proc. of 7th Intern. Vac. Congr. and 3rd Intern. Conf. on Solid Surf., Vienna, 1977, (F.Berger and Sorne, Vienna, 1977) p.1533.

17) E.H.Hirsch and I.K.Varga, Thin Solid Films, 52(1978) p.445.

18) Y.Namba and T.Mori, Thin Solid Films, 39(1976) p.119.

19) M.Marinov and D.Dobrev, Thin Solid Films, 42(1977) p.265.

20) D.G.Teer and B.L.Delcea, Proc. of Intern. Conf. on Ion Plating and Allied Techniques (IPAT '77), Edinburgh, 1977, (CEP Consultants Ltd., Edinburgh, 1977) p.58.

21) T.Takagi, I.Yamada, M.Kunori and S.Kobiyama, Proc. of 2rd Intern. Conf. on Ion Sources, Vienna, 1972, (SAGE, Vienna, 1972) p.790.

22) T.Takagi, I.Yamada and A.Sasaki, Thin Solid Films, 39(1976) p.207.

23) T.Takagi, I.Yamada and A.Sasaki, Proc. of Intern. Conf. on Low Energy Ion Beams, Salford, 1977, Inst. Phys. Conf. Ser. No.38(1978) Chap.3, p.142.

24) T.Takagi, I.Yamada and A.Sasaki, Thin Solid Films, 45(1977) p.569

25) A.E.Berkowitz and W.H.Meiklejohn, IEEE Trans. on Magn., MAG-11(1975) p.996.

26) K.Lee, J. Vac. Sci. Technol., 10(1973) p.631.

27) D.Chen, Appl. Optics, 13(1974) p.767.

28) J.D.Zook, Appl. Oct., 13(1974) p.875.

29) L.Mayer, J. Appl. Phys., 29(1958) p.1003.

30) J.T.Chang, J.F.Dillon,Jr and U.F.Gianola, J. APPL. Phys., 36 (1965) p.1110.

31) R.E.MacDonald and J.W.Beck, J. Appl. Phys., 40(1969) p.1429.

32) R.P.Hunt, IEEE Trans. on Magn., MAG-5(1969) p.700.

33) J.C.Suits, IEEE Trans. on Magn., MAG-8(1972) p.95.

34) M.J.Feisen, IEEE Trans. on Magn., MAG-4(1968) p.153.

35) B.D.Silverman, J. Appl. Phys., 43(1972) p.5163.

36) E.Feldtkeller, IEEE Trans. on Magn., MAG-8(1972) p.481.

37) R.Cohen and S.Mezrich, RCA Rev., 33(1972) p.54.

38) T.Takagi, I.Yamada and A.Sasaki, J. Vac. Sci. Technol., 12 (1975) p.1128.

39) T.Takagi, I.Yamada and A.Sasaki, Technical Digest of Intern. Electron Devices Meeting, Washington D.C., 1976. p.605.

40) T.Takagi, I.Yamada and A.Sasaki, Proc. of Intern. Conf. on Ion Plating and Allied Techniques (IPAT '77), Edinburgh, 1977, (CEP Consultants Ltd., Edinburgh, 1977) p.50.

41) T.Takagi, I.Yamada, A.Sasaki, S.Itoh, M.Ozawa, M.Kodama, K.Tominaga and T.Hattori, Proc. of 7th Intern. Vac. Congr. and 3rd Intern. Conf. on Solid Surf., Vienna, 1977, (F.Berger and Sohne, Vienna, 1977) p.1603.

42) T.Takagi, I.Yamada and A.Sasaki, Proc. of 7th Intern. Vac. Congr. and 3rd Intern. Conf. on Solid Surf., Vienna, 1977, (F.Berger and Sohne, Vienna, 1977) p.1915.

43) T.Takagi, I.Yamada and A.Sasaki, Proc. of 6th Intern. Conf. on Molecular Beams, Noordwijkerhout, 1977, p.53.

44) T.Takagi, I.Yamada and A.Sasaki, Proc. of Intern. Conf. on Low Energy Ion Beams, Salford, 1977, Inst. Phys. Cond. Ser. No.38 (1977) Chap.5, p.229.

45) T.Takagi, I.Yamada, K.Matsubara and H.Takaoka, J. Cryst. Growth, 45(1978) p.318.

46) I.Yamada, K.Matsubara, M.Kodama, M.Ozawa and T.Takagi, J. Cryst. Growth, 45(1978) p.326.

47) T.Takagi, I.Yamada and A.Sasaki, IEE Trans. on Solid State and Electron Devices, 2 (Special Issue) (1978) p.40.

48) T.Takagi, I.Yamada and K.Matsubara, Thin Solid Films, 58 (1979) p.9.

49) K.Matsubara, I.Yamada, N.Nagao, K.Tominaga and T.Takagi, Surf. Sci., 86(1979) p.290.

50) T.Takagi, K.Matsubara, N.Kondo, K.Fujii and H.Takaoka, Jpn. J. Appl. Phys., 19(1980) Supple. 19-1, p.507.

51) T.Takagi, K.Matsubara and H.Takaoka, J. Appl. Phys., 51 (1980) p.5419.

52) I.Yamada, F.W.Saris, T.Takagi, K.Matsubara, H.Takaoka and S.Ishiyama, Jpn. J. Appl. Phys., 19(1980) L.181.

53) J.B.Theeten, R.Madar, A.Mircea-Roussel, A.Rocher and G.Lawrence, J. Cryst. Growth, 37(1979) p.317.

54) K.Morimoto, H.Watanabe and S.Itoh, J. Cryst. Growth, 45 (1978) p.334.

55) A.E.T.Kuiper, G.E.Thomas and W.J.Shouter, J. Cryst. Growth, 45(1978) p.332.

56) S.B.Sample, R.Bullini and D.A.Decher, Proc. of 11th Symp. on Electron, Ion and Laser Technol., 1971, (IEEE Catalog No.71C23-ED) p.359.

57) R.Clampitt, L.Gowland and K.L.Aitken, Proc. on Intern. Conf. on Ion Plating and Allied Techniques (IPAT '77), Edinburgh, 1977, (CEP Consultant Ltd., Edinburgh, 1977) p.70.

58) R.Clampitt and D.K.Jefferies, Proc. of Intern. Conf. on Low Energy Ion Beams, Salford, 1977, Inst. Phys. Conf. Ser. No.38. (1978) Chap.1, p.12.

59) R.Clampitt, Thin Solid Films, 58(1979) p.129.

60) R.F.C.Fanow, A.G.Cullins, A.J.Grant, G.R.Jones and R.Clampitt, Thin Solid Films, 58(1979) p.189.

61) T.Takagi, I.Yamada, K.Matsubara and H.Takaoka, Proc. of 2nd Intern. Meeting on Small Particles and Inorganic Clusters, Lausanne, 1980, p.43 and p.94.

62) F.Bottiglion, J.Coutant and M.Fois, Phys. Rev., A6(1972) p.1830.

63) I.Yamada, H.Inokawa, H.Usui and T.Takagi, Proc. of 4th Symp. on Ion Source and Ion Appl. Technol., Tokyo, 1980, p.69.

64) T.Takagi, K.Matsubara, H.Takaoka and I.Yamada, Proc. of Intern. Conf. on Ion Plating and Allied Techniques (IPAT '79), London, 1979, (CEP Consultants Ltd., Edinburgh, 1979) p.174.

65) D.Chen, G.N.Otto and F.M.Schmit, IEEE Trans. on Magn., MAG-9(1973) p.66.

66) A.F.Andresen, J.E.Engebretsen and J.Rifsnes, Acta. Chem. Scand., 26(1972) p.175.

67) B.W.Roberts, Phys. Rev., 104(1956) p.607.

68) A.F.Andresen, Acta. Chem. Scand., 21(1967) p.1543.

69) C.Gullaud, J. Phys. Radium, 12(1951) p.143.

70) Y.Takeno and Y.Iwama, Jpn. J. Appl. Phys., 18(1979) p.269.

71) W.K.Unger and E.Wolfgang, J. Appl. Phys., 42(1971) p.4221.

72) P.Dekker, P.W.Jedeloo and S.Middlehoek, IEEE Trans. on Magn., MAG-10(1974) p.591.

73) P.Dekker and H.A.M. van den Berg, IEEE Trans. on Magn., MAG-10(1974) p.595.

74) H.J.Williams, R.C.Sherwood and O.L.Boothby, J. Appl. Phys., 28(1957) p.445.

75) L.Mayer, J. Appl. Phys., 29(1958) p.1454.

76) D.O.Smith, IEEE Trans. on Magn., MAG-3(1967) p.594.

77) R.L.Aagard, D.Chen, R.W.Honebrink, G.N.Otto and F.M.Schmit, IEEE Trans. on Magn., MAG-4(1968) p.412.

78) R.Langlet, B.Carre and J.P.Pivot, IEEE Trans. on Magn., MAG-9(1973) p.401.

79) D.Chen, J. Appl. Phys., 42(1971) p.3625.

80) L.Mayer, J. Appl. Phys., 31(1960) p.346.

81) Y.Iwama, U.Mizutani and F.B.Humphrey, IEEE Trans. on Magn., MAG-8(1972) p.487.

82) G.Lewicki and J.E.Guisinger, J. Appl. Phys., 44(1973) p.2361.

83) S.Honda and T.Kusuda, J. Appl. Phys., 45(1974) p.2689.

84) S.Esho, S.Noguchi and M.Nagao, J. Phys. Soc. of Jpn., 33 (1972) p.1718.

85) L.Mayer, J. Appl. Phys., 31(1960) p.384S.

86) S.Honda, Y.Hosokawa, S.Konishi and T.Kusuda, Jpn. J. Appl. Phys., 12(1973) p.1028.

87) A.Shibukawa, A.Katsui and K.Egashira, Jpn. J. Appl. Phys., 15(1976) p.1915.

88) K.Egashira, A.Katsui and A.Shibukawa, Tech. Rep. of "Shingakukai", MR74-14(1974) p.27.

89) K.Egashira and T.Yamada, J. Appl. Phys., 45(1974) p.3643.

90) G.Lewicki and J.E.Guisinger, Appl. Phys. Lett., 16(1970) p.240.

91) A.A.Thiele, J. Appl. Phys., 41(1970) p.1139.

92) S.Honda, T.Nomura and T.Kusuda, IEEE Trans. on Magn., MAG-9 (1973) p.467.

93) A.H.Bobeck, Bell Syst. Tech. J., 46(1967) p.1901.

94) A.V.Lugt, Proc. of IEEE, 62(1974) p.1300.

95) J.C.Suits, G.B.Street, K.Lee and J.B.Goodenough, Phys. Rev., B10(1974) p.120.

96) H.Göbel et al., Phys. Stat. Sol., (a)35(1976) p.89.

97) L.Néel, "Le Magnetism", vol.2, 1940.

98) R.C.Lecraw and R.D.Pierce, AIP Conf. Proc., 5(1972) p.200.

99) G.B.Street, J.C.Suits and K.Lee, Solid State Commum., 14 (1974) p.33.

100) A.Brenner, D.E.Couch and E.K.Williams, J. Res. National Bureau of Standards, 44(1950) p.109.

101) H.O.Hooper and A.M.deGraaf(editors); "Amorphous Magnetism", Plenum Press, New York, (1973).

102) P.L.Maitre-Pierre, J.Appl.Phys., 40(1969) p.4826.

103) T.E.Sharon and C.C.Tsuei, Phys. Rev., B5(1972) p.1047.

104) G.S.Cargill, J. Appl. Phys., 41(1970) p.12.

105) G.S.Cargill and R.W.Cochrane, ref. 101), (1973) p.313.

106) S.Fujima, Jpn. J. Appl. Phys., 6(1967) p.305.

107) S.Mader and A.S.Norwick, Appl. Phys. Lett., 7(1967) p.57.

108) J.J.Rhyne, S.J.Pickart and H.A.Alperin, 19th AIP Conf. Proc., No.18, Part 1, Boston, (1973) p.563.

109) J.J.Rhyne and T.R.McGuire, IEEE Trans. on Magn., MAG-8 (1972) p.105.

110) P.Chaudhari, J.J.Cuomo and R.J.Gambino, IBM J. Res. Dev., 17(1973) p.66.

111) G.E.Roberts, W.L.Wilson Jr and H.C.Bourne Jr, IEEE Trans. on Magn., MAG-13 (1977) p.1535.

112) R.J.Gambino, J.Ziegler and J.J.Cuomo, Appl. Phys. Lett., 24(1974) p.99.

113) R.C.Taylor, J. Appl. Phys., 47(1976) p.1164.

114) S.Esho, J. Appl. Phys., 50(1979) p.1006.

115) J.Orehotsky, K.Schröder, J. Appl. Phys., 43(1972) p.2413.

116) A.G.Dirks and H.J.Leamy, J. Appl. Phys., 49(1978) p.1735.

117) N.S.Gingrich, Rev. Mod. Phys., 15(1943) p.90.

118) I.L.Karle and J.Karle, J. Chem. Phys., 17(1949) p.1052.

119) C.H.MacGillvry, G.D.Rieck and K.Lonsdale(editors): "International Tables for X-ray Crystallography", vol.III, The Kynoch Press, Birmingham, England, (1968).

120) Y.Nishihara, T.Katayama, Y.Yamaguchi, S.Ogawa and T.Tsushima, Jpn. J. Appl. Phys., 17(1978) p.1083.

121) S.Honda, M.Ohkoshi and T.Kusuda, Proc. of 3rd Intern. Conf. on Ferrites, (1981).

122) R.K.Wangsness, Phys. Rev., 86(1952) p.146.

123) R.K.Wangsness, Phys. Rev., 91(1953) p.1085.

124) N.Tsuya, Prog. Theor. Phys., 7(1952) p.263.

125) P.Hansen and M.Urner-Wille, J. Appl. Phys., 50(1979) p.7471.

126) T.Sato, M.Sakata and H.Nosé, J Phys. Soc. of Jpn., 50(1981) p.2246.

LIST OF PUBLICATION

I. PAPERS

1) T.Takagi, K.Matsubara, N.Kondo, K.Fujii and H.Takaoka:
"Magnetooptical Properties of MnBi Films Prepared by Ionized-Cluster Beam Deposition Technique",
Proc. of the 11th Conf. (1979 International) on Solid State Devices, Tokyo, 1979; Jpn. J.Appl. Phys., 19 (1980) Suppl. 19-1, p.507-p.511.

2) N.Kondo, K.Matsubara and T.Takagi:
"Structural and Magnetic Properties of Gd-Fe Thin Films Prepared by Ionized Cluster Beam (ICB) Technique",
J. Magn. Soc. of Jpn., vol.5, No.2, (1980) p.105-p.108.

3) N.Kondo, M.Ohura, K.Matsubara and T.Tkagi:
"Structural and Magnetic Properties of Amorphous GdFe-Bi Magnetic Films Prepared by ICB Technique",
J. Magn. Soc. of Jpn., vol.6, No.2, (1982) p.

II. PROCEEDINGS

1) K.Matsubara, I.Yamada, N.Kondo and T.Takagi:
"Magnetic Properties of MnBi Thin Films Prepared by Ionized-Cluster Beam Deposition",
Preprint of International Conf. of Vapour Growth and Epitaxy, (1978) p.183-p.184.

2) K.Matsubara, N.Kondo, K.Fujii and T.Takagi:
"Formation of MnBi Thin Films by Multitype Ionized-Cluster Beam Deposition",
J. of the Jpn. Association of Crystal Growth, vol.5, No.3, (1978) p.56.

3) K.Matsubara, N.Kondo, K.Fujii, H.Takaoka and T.Takagi:
"Domain Growing Mechanism and Curie Point Writing of MnBi Films Prepared by Multitype Ionized-Cluster Beam Technology", Proc. of 3rd Symp. on Ion Sources and Application Technology, Tokyo, (1979) p.131-p.132.

4) N.Kondo, K.Matsubara and T.Takagi:
"Crystallographic and Magnetic Properties of $Mn_5Ni_2Bi_4$ Thin Films Prepared by ICB Technique",
Proc. of the 4th Symp. on Ion Sources and Ion Application Technology, Tokyo, (1980) p.133-p.136.

LIST OF TECHNICAL REPORTS

1) N.Kondo, K.Matsubara, I.Yamada and T.Takagi:
"Formation of MnBi Thin Films by Ionized-Cluster Beam Technique", The Fall Meeting of JSAP, Paper No. 5p-S-10, (1978) p.373.

2) K.Matsubara, N.Kondo, K.Fujii and T.Takagi:
"Evaluation of MnBi Films Prepared by Ionized Cluster Beam Deposition Technique", Proc. of the 2nd Conf. on Magn., Paper No. 22pB-11, (1978)

3) K.Fujii, N.Kondo, K.Matsubara and T.Takagi:
"Properties of $Mn_5Ni_2Bi_4$ Films Prepared by Ionized Cluster Beam Deposition Technique", Proc. of the 3rd Conf. on Magn., Paper No. 25pB-1, (1979) p.100.

4) N.Kondo, K.Fujii, K.Matsubara and T.Takagi:
"Formation of Co-Doped MnBi Films Using Ionized Cluster Beam Deposition Technique", Proc. of the 3rd Conf. on Magn., Paper No. 25pB-2, (1979) p.101.

5) N.Kondo, K.Fujii, K.Matsubara and T.Takagi:
"Formation of $Mn_5Ni_2Bi_4$ Thin Films Prepared by ICB Technique", The Spring Meeting of JSAP, Paper No. 1p-B-8, (1980) p.277.

6) N.Kondo, K.Matsubara and T.Takagi:
"Preparation of Amorphous Gf-Fe Films by ICB Technique", Proc. of the 4th Conf. on Magn., Paper No. 4pB-3, (1980) p.49.

7) N.Kondo, K.Matsubara and T.Takagi:
"Magnetic Properties of Amorphous Gd-Fe Films by ICB Technique", Proc. of the 4th Conf. on Magn., Paper No. 4pB-4, (1980) p.50.

8) N.Kondo, K.Matsubara and T.Takagi:
"Structural Analysis of Amorphous Gd-Fe Films Prepared by ICB Technique", The Spring Meeting of JSAP, Paper No. 31a-E-9, (1981) p.279.

9) N.Kondo, K.Matsubara and T.Takagi:
"Formation and Magnetic Properties of Gd-Fe Thin Films Prepared by ICB Technique", Paper of Technical Group on Magnetics of IEEEJ, Paper No. MAG-81-3, (1981) p.21-p.28.

10) N.Kondo, M.Ohura, K.Matsubara and T.Takagi:
"Structural Analysis of Bi-doped GdFe Amorphous Films Prepared by Ionized-Cluster Beam", Proc. of the 5th Conf. on Magn., Paper No. 20pB-7, (1981) p.45.

11) K.Matsubara, H.Takaoka, N.Kondo and T.Takagi:
"A Study on the Growth Mechanism of Preferentially Oriented Thin Films", The Fall Meeting of JSAP, Paper No. 18a-W-9, (1980) p.242.

12) N.Kondo, M.Ohura, K.Matsubara and T.Takagi:
"Structural and Magnetic Properties of Bi-doped Amorphous GdFe Films Prepared by ICB Technique", The Spring Meeting of JSAP, Paper No. 3p-D-13, (1982) p.

---

*JSAP (The Japan Society of Applied Physics)

*IEEJ (The Institute of Electrical Engineers of Japan)